UNCLASS

SECURITY CLASSIFICATION OF THIS PAGE (When Data Entered)

REPORT DOCUMENTATION PAGE

READ INSTRUCTIONS BEFORE COMPLETING FORM

1. REPORT NUMBER: AFIT/CI/NR-84-28T
2. GOVT ACCESSION NO.
3. RECIPIENT'S CATALOG NUMBER

4. TITLE (and Subtitle): Time-Dependent Oscillations In A CW HF Chemical Laser Unstable Resonator
5. TYPE OF REPORT & PERIOD COVERED: THESIS/DISSERTATION
6. PERFORMING ORG. REPORT NUMBER

7. AUTHOR(s): Steven Wayne Towsend
8. CONTRACT OR GRANT NUMBER(s)

9. PERFORMING ORGANIZATION NAME AND ADDRESS: AFIT STUDENT AT: University of Illinois
10. PROGRAM ELEMENT, PROJECT, TASK AREA & WORK UNIT NUMBERS

11. CONTROLLING OFFICE NAME AND ADDRESS: AFIT/NR, WPAFB OH 45433
12. REPORT DATE: 1984
13. NUMBER OF PAGES: 63

14. MONITORING AGENCY NAME & ADDRESS(if different from Controlling Office)
15. SECURITY CLASS. (of this report): UNCLASS
15a. DECLASSIFICATION/DOWNGRADING SCHEDULE

16. DISTRIBUTION STATEMENT (of this Report)

APPROVED FOR PUBLIC RELEASE; DISTRIBUTION UNLIMITED

17. DISTRIBUTION STATEMENT (of the abstract entered in Block 20, if different from Report)

18. SUPPLEMENTARY NOTES

APPROVED FOR PUBLIC RELEASE: IAW AFR 190-1

LYNN E. WOLAVER
Dean for Research and Professional Development
AFIT, Wright-Patterson AFB OH

19. KEY WORDS (Continue on reverse side if necessary and identify by block number)

20. ABSTRACT (Continue on reverse side if necessary and identify by block number)

ATTACHED

DD FORM 1 JAN 73 1473 EDITION OF 1 NOV 65 IS OBSOLETE

UNCLASS

SECURITY CLASSIFICATION OF THIS PAGE (When Data Entered)

ABSTRACT

The multi-line performance of a cw HF chemical laser was measured as a function of the SF_6 and H_2 flow rates, pressure and resonator type. The Blaze II and MNORO3 cw chemical laser computer codes gave reasonable agreement with the experimental data as the flow rates and pressure were varied. Total power and beam diameter increased as the pressure decreased. The data indicate the occurrence of a near resonant energy transfer from v=2, J=3, 4 to v=2, J=14 with a subsequent rotational cascade to v=2, J=11. The amplitude, frequency and Fresnel number dependence of the time-dependent oscillations which were predicted to occur on lines whose saturated gain does not fill the unstable resonator were measured. The time-dependent oscillations had a period of about 40 ns independent of flow rates, do not occur for Fresnel numbers less than 1.5 and their amplitudes increased as the fraction of the resonator filled by the saturated gain of the oscillating line decreased. The period of the time-dependent oscillations was determined by the resonator magnification. There was a strong cascade coupling between the oscillating 2→1 and 1→0 lines. The a priori prediction of these characteristics of the time-dependent oscillations by the MNORO3UR computer model was in agreement with the data. A 7 ns oscillation, which was probably a mode beat of the laser, was superimposed on top of the 40 ns oscillation. The time-dependent oscillations occurred in both two and three dimensional unstable resonators.

TIME-DEPENDENT OSCILLATIONS IN A CW HF CHEMICAL LASER UNSTABLE RESONATOR

BY

STEVEN WAYNE TOWNSEND

B.S., University of Illinois, 1983

THESIS

Submitted in partial fulfillment of the requirements
for the degree of Master of Science in
Aeronautical and Astronautical Engineering
in the Graduate College of the
University of Illinois at Urbana-Champaign, 1984

Urbana, Illinois

UNIVERSITY OF ILLINOIS AT URBANA-CHAMPAIGN

THE GRADUATE COLLEGE

MAY 14, 1984

WE HEREBY RECOMMEND THAT THE THESIS BY

STEVEN WAYNE TOWNSEND

ENTITLED TIME-DEPENDENT OSCILLATIONS IN A

CW HF CHEMICAL LASER UNSTABLE RESONATOR

BE ACCEPTED IN PARTIAL FULFILLMENT OF THE REQUIREMENTS FOR

THE DEGREE OF MASTER OF SCIENCE

Lee W. Casperson
Director of Thesis Research

Harry H. Hilton
Head of Department

Committee on Final Examination†

Chairman

† Required for doctor's degree but not for master's.

O-517

TABLE OF CONTENTS

I. INTRODUCTION

This study is part of an integrated theoretical and experimental investigation of the nonlinear interactions which may occur between the chemical kinetics, the fluid dynamics and the optical resonator of a cw fluid flow laser. The objectives of this study were to measure the frequency and amplitude of the time-dependent oscillations which have been predicted to occur in cw lasers employing unstable resonators to extract power[1,2,3]. These time-dependent oscillations in cw power, which were shown to be a consequence of rotational nonequilibrium, may develope on lines whose saturated gain zone does not fill the unstable resonator. For these oscillations to occur, the Fresnel number of the resonator must be greater than 1.5, the amplitude of the oscillation is determined by the fraction of the resonator filled by the saturated gain zone of the oscillating line, and the frequency of the oscillation is determined by the geometric outcoupling ratio and the fraction of the resonator filled by the saturated gain of the oscillating line. The length of the saturated gain zone of the lasing line was shown to be independent of the size of the resonator[1,2]. Based on these results, the success of the experimental study depended upon the ability to design an unstable resonator in which the saturated gain zone of one or more of the peak power lines does not reach further into the unstable resonator than the center line. The importance of this point is illustrated by a previous experiment[4] which obtained a null result (no oscillations were observed) because the saturated gain zone of the lasing line filled the resonator. The design of the unstable resonator thus depends upon the ability to predict the length of the saturated gain zones for the lasing lines for the laser to be used

in the experimental study.

In the present study, the frequency and amplitude of the time-dependent oscillations which occur in a cw laser employing a confocal, unstable resonator were measured. Unstable resonator modeling calculations[3] indicated that for a resonator with Fresnel number large enough for the oscillations to occur, at a pressure of 10 to 12 torr, the saturated gain zones of the laser used in the experiments were not long enough for lasing to occur. Thus, to stretch the gain zones, the laser was run at the lowest pressure obtainable in the cavity (about 5 torr).

A low pressure stable resonator study was performed to provide a data base for verifying the computer model as a function of pressure. Comparison of the stable resonator data and MNORO3 results for both high and low pressure conditions showed that the model agrees with the data as flow rates, cavity losses and pressure are varied. In addition, the minimum in the spectra at $P_2(11)$ occurred in the low pressure as well as in the high pressure[5,6,7] data. However, the lines $P_2(10)$ to $P_2(12)$ were weaker in the low pressure cases than in the high pressure cases. This supports the interpretation[6,7] of the minima as evidence for a kinetic effect, namely a near resonant energy transfer from v=3, J=3, 4 to v=2, J=14 with a subsequent rotational cascade to v=2, J=11. The flow rates which resulted in the longest saturated gain zones (largest beam diameter) were chosen for the unstable resonator experiments.

To obtain an a priori estimate of the periods and amplitudes of the time-dependent oscillations, the MNORO3UR code[3] was run for these flow rates at 5.4 torr. The results of the calculations indicated that the oscillations would have a period of approximately 40 ns independent of flow

rate and Fresnel number. Th. experiments were performed with a 50% geometric outcoupled, confocal, unstable resonator. A variable slit scraper mirror permitted the Fresnel number to vary from 0 to 35.7. Both low and high pressure data were obtained. As predicted by the MNORO3UR calculations, the period of the time-dependent oscillations varied from 33 to 47 ns and their amplitude increased from 10% to 80% as the fraction of the resonator filled by the saturated gain of the oscillating line decreased. There was a strong cascade coupling between the oscillating 1→0 and 2→1 lines. A 7 ns oscillation, which was probably a mode beat of the laser, was superimposed on top of the 40 ns oscillation. As predicted by the a priori MNORO3UR calculations, for Fresnel numbers less than 1.5, no oscillations were observed on lines whose saturated gain did not fill the unstable resonator. No oscillations were observed when the laser cavity pressure was in the 10 to 12 torr range. This may be a consequence of either the increased rotational relaxation rate which occurs as the pressure increases, or the saturated gain zones may have been too short, which results in the Fresnel number (based on the saturated gain zone lengths) being too small for the time-dependent oscillations to occur.

Time-dependent oscillations on lines whose saturated gain did not fill the unstable resonator were also observed using a scraper mirror with a rectangular hole in it. In this case, the resonator acts as a three dimensional resonator rather than as a strip resonator as was the case when the slit scraper mirror was used. The periods of the time-dependent oscillations were 40 ns and their amplitudes increased as the fraction of the resonator filled by the saturated gain decreased. Since the magnification of the two and three dimensional resonators was the same, the

data indicated that the frequency of the oscillations is determined by the resonator magnification rather than the geometric outcoupling ratio.

In Section II, the low pressure stable resonator data are presented and compared to the Blaze II and MNORO3 calculations and to the corresponding high pressure stable resonator data. In Section III, the data on the time-dependent oscillations on lines whose saturated gain zones do not fill the unstable resonator are presented and compared to the MNORO3UR calculations. Several conclusions and recommendations for future study are given in Section IV.

II. LOW PRESSURE, STABLE RESONATOR PERFORMANCE

Since the unstable resonator modeling calculations[3] indicated that the occurrence of the time-dependent oscillations on lines whose saturated gain does not fill the unstable resonator is Fresnel number dependent and that, for the conditions of the high pressure (11 torr) Run 36, lasing may not occur for a resonator whose Fresnel number is large enough that the time-dependent oscillations should occur, the laser was run at the lowest pressure obtainable in the cavity (about 5 torr) in order to stretch the gain zones. To provide a data base for baselining the computer models, stable resonator power versus x_c data was obtained for the six SF_6 and H_2 flow rate combinations with the vacuum control valve wide open. For the x_c of peak power, beam diameters, pressure and spectra were measured in the same manner as in the previous high pressure laser performance studies[2,5,6,7]. These data were taken with the 56% mirror and two 4 cm CaF_2 Brewster windows, which corresponded to an effective reflectivity of 39%[6,7]. The Blaze II[8] computer model is compared to the data as a function of cavity pressure in Fig. 1. The only parameter changed in the model for these calculations was the initial pressure at the inlet of the laser cavity. From Fig. 1, it is seen that the model gives very good agreement with the data over the entire pressure range accessible with our vacuum system.

The low pressure stable resonator data are summarized in Table 1. From Table 1, it is seen that the Blaze II and MNOR03[9] results are in good agreement with the data. The corresponding high pressure stable resonator results are summarized in Table 2[6,7]. Comparison of the low and high pressure stable resonator data shows that the beam diameter and total power

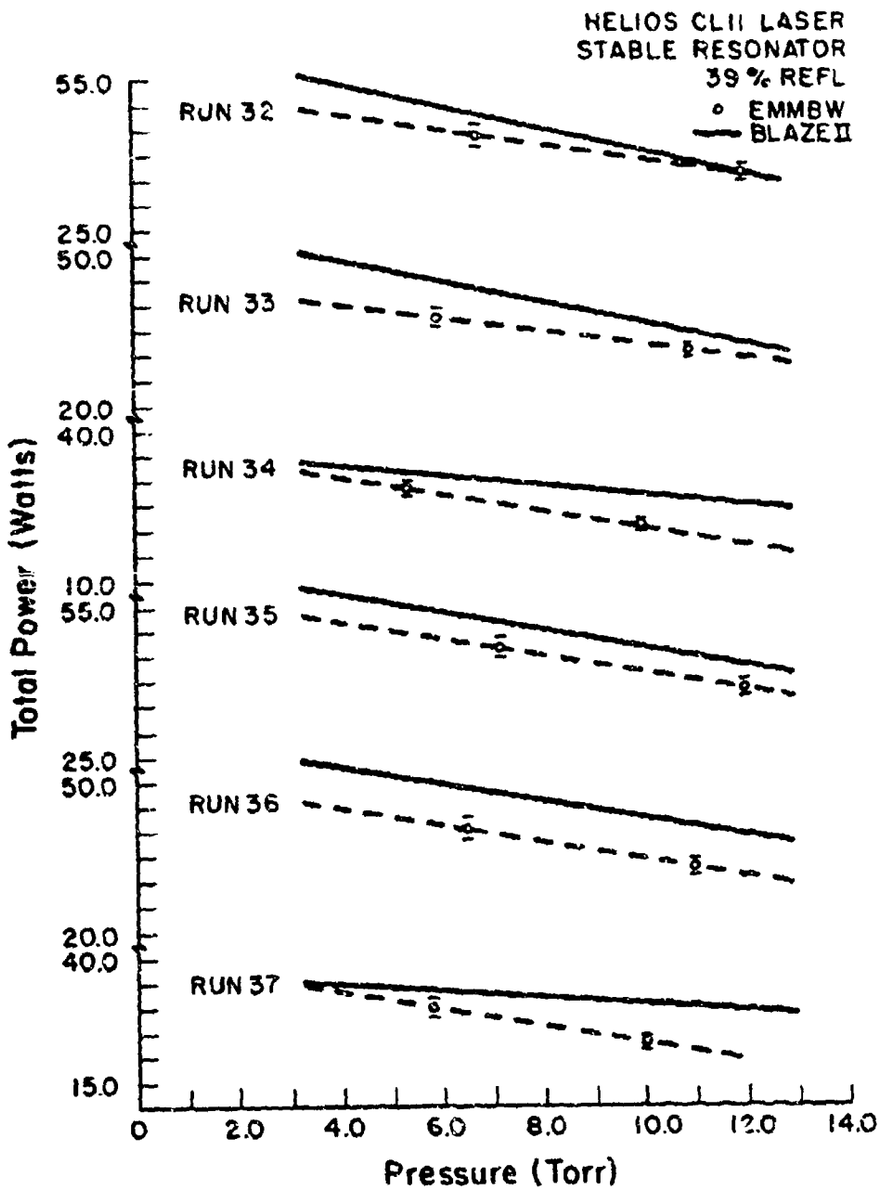

Figure 1. Comparison of experimental and predicted laser performance versus pressure for the Helios CL II laser when Brewster windows are used with the 56% reflective outcoupler. EMMBW denotes external mirror mounts with two Brewster windows data; the effective cavity reflectivity was 39%.

RUN NO.	32	33	34	35	36	37
$\dot{m}_{SF_6}$, gm/sec	1.36	1.01	0.67	1.36	1.01	0.67
$\dot{m}_{H_2}$, gm/sec	0.0375	0.0375	0.0375	0.0545	0.0545	0.0545
P, Torr	6.75	6.0	5.40	7.20	6.48	5.83
% SF_6 Dissoc.	3.3	4.0	4.0	3.3	4.0	4.0
Initial T, °K	500	450	450	500	450	450
H_2 mixing length, cm	3.0	3.5	4.0	3.0	3.5	4.0
P_T, watts						
Data	43.7	37.5	28.2	46.2	40.2	29.6
Blaze II	48.5	45.5	31.5	52.6	49.2	33.3
MNORO3		45.9	31.6		49.3	33.6
P_{10}/P_T						
Data	0.481	0.512	0.468	0.493	0.511	0.472
Blaze II	0.504	0.493	0.485	0.501	0.492	0.486
MNORO3		0.504	0.494		0.501	0.493
Beam Dia., mm						
Data	4.90	5.00	5.10	4.60	4.50	4.50
Blaze II	5.30	5.60	5.70	4.10	4.30	4.30
MNORO3		5.50	5.90		4.80	4.70

Table 1. Comparison of the low pressure Blaze II and MNORC3 results with the data for the Helios CL II laser with a stable resonator with external mirror mounts and 4 cm CaF_2 Brewster windows which result in a 39% effective reflectivity. The primary mixing length is 0.001 cm for all cases.

RUN NO.	32	33	34	35	36	37
$\dot{m}_{SF_6}$, gm/sec	1.36	1.01	0.67	1.36	1.01	0.67
$\dot{m}_{H_2}$, gm/sec	0.0357	0.0357	0.0357	0.0545	0.0545	0.0545
P, Torr	12.2	11.1	10.0	12.1	11.0	10.0
% SF_6 Dissoc.	3.3	4.0	4.0	3.3	4.0	4.0
Initial T, °K	500	450	450	500	450	450
H_2 mixing length, cm	3.0	3.5	4.0	3.0	3.5	4.0
P_T,watts						
Data	35.5	30.5	20.5-20.75	38.0	32.5	22.0-22.25
Blaze II	33.4	34.0	27.6	41.9	41.2	31.1
P_{10}/P_T						
Data	0.530	0.483	0.472	0.520	0.531	0.474
Blaze II	0.539	0.519	0.502	0.523	0.510	0.498
Beam Dia., mm						
Data	3.39	3.43	2.91	3.21	3.06	3.09
Blaze II	3.30	3.40	3.50	2.80	2.80	2.80

Table 2. Summary of the high pressure data and Blaze II results for the Helios CL II laser with a stable resonator with external mirror mounts and 4 cm CaF_2 Brewster windows which result in a 39% effective reflectivity. The primary mixing length is 0.001 cm for all cases.

increased for all six cases when the cavity pressure was decreased. For the low pressure case, the diameter increased 43% to 47% except for Run 34. The low pressure Run 34 beam diameter increased 75%. Total power increased between 21% and 24% for Runs 32, 33, 35 and 36, 36% to 38% for Run 34 and 33% to 34% for Run 37. The total power increases are evidence that the HF deactivation rate decreased due to the lower pressure. Runs 34 and 37 had an additional 10% to 15% increase in total power compared to the other cases. The fraction of the power in the 1→0 vibrational band did not change significantly for any of the cases when the pressure was decreased.

The power spectral distributions for the six low pressure cases are shown in the order of increasing SF_6 flow rate for a fixed H_2 flow rate in Figs. 2 and 3. From these figures, it is seen that at both the low and high H_2 flow rates, the power spectral distribution shifted toward higher J's as the SF_6 flow rate increased. Figures 4 and 5 show the power spectral distributions for the corresponding high pressure cases[6,7], which also show the same shift to higher J's. The shift of the power spectral distribution toward higher J's as the SF_6 flow rate increased for a fixed H_2 flow rate is caused by the increase in the temperature which accompanies the increased heat released due to the increased F atom flow rate[2,5].

Comparison of the high and low pressure power spectral distributions for fixed flow rates shows that the power spectral distributions shifted to lower J's as the pressure decreased. Since the rotational relaxation rate is proportional to pressure squared, the shift of the power spectral distribution toward lower J's as the pressure decreased is a consequence of the decreased rotational relaxation which occurs at low pressures.

MNORO3 power spectral distributions are compared to the low pressure

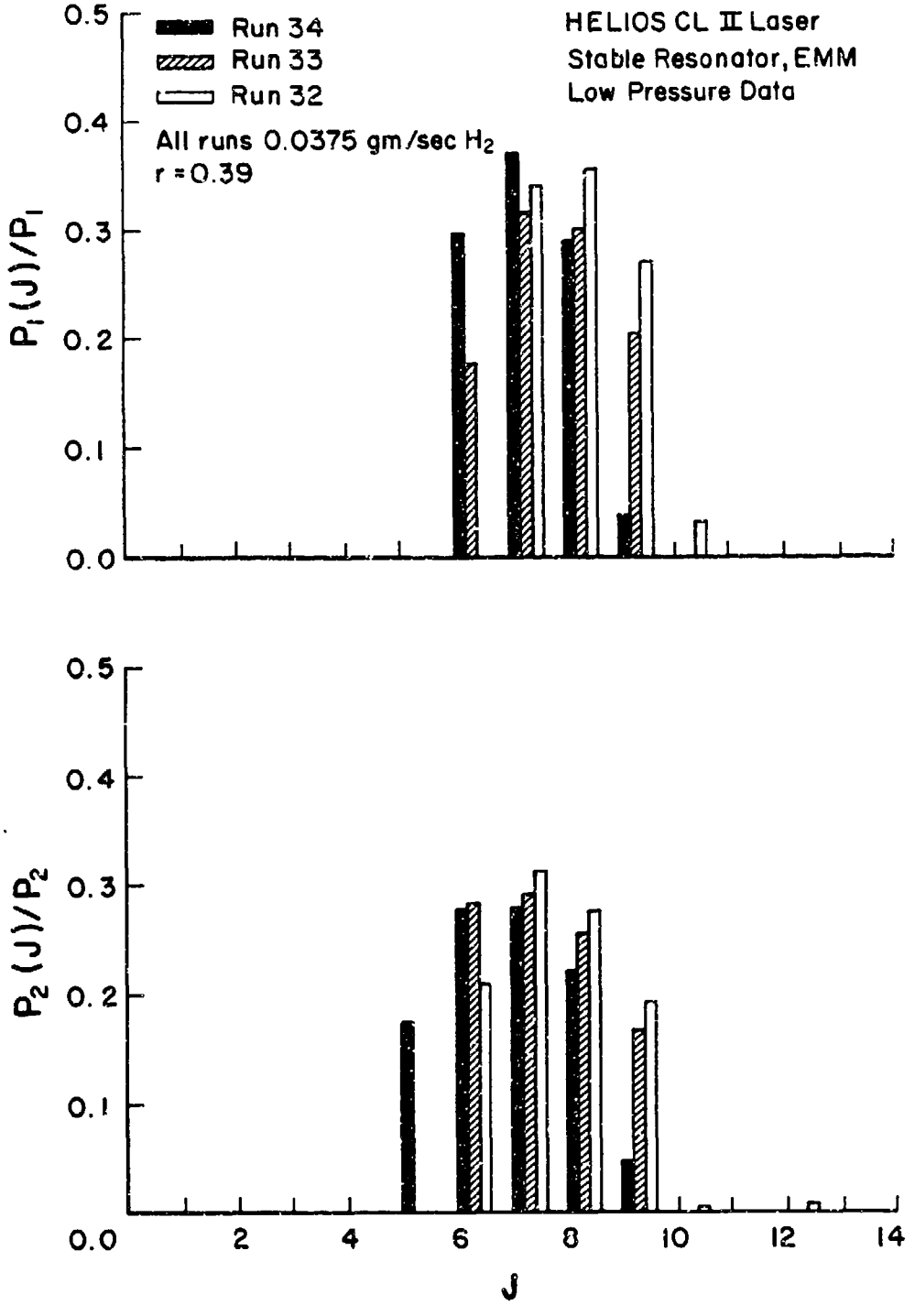

Figure 2. Experimental low pressure stable resonator power spectral distributions for the Helios CL II laser for three different SF_6 flow rates. $\dot{m}_{He}$ = 0.078 gm/sec and $\dot{m}_{O_2}$ = 0.28 gm/sec. r = 0.39.

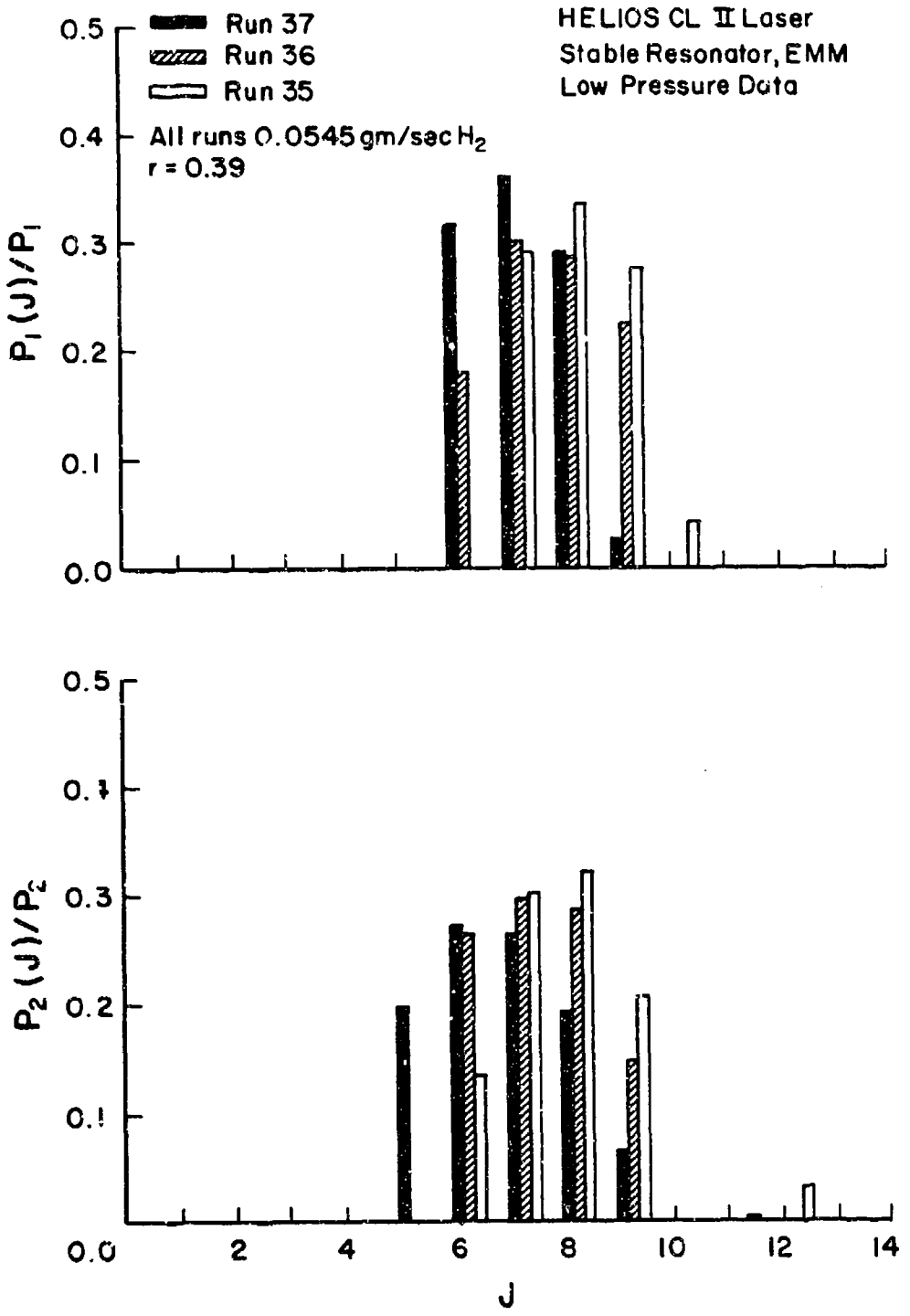

Figure 3. Experimental low pressure stable resonator power spectral distributions for the Helios CL II laser for three different SF_6 flow rates. $\dot{m}_{He}$ = 0.078 gm/sec and $\dot{m}_{O_2}$ = 0.28 gm/sec. r = 0.39.

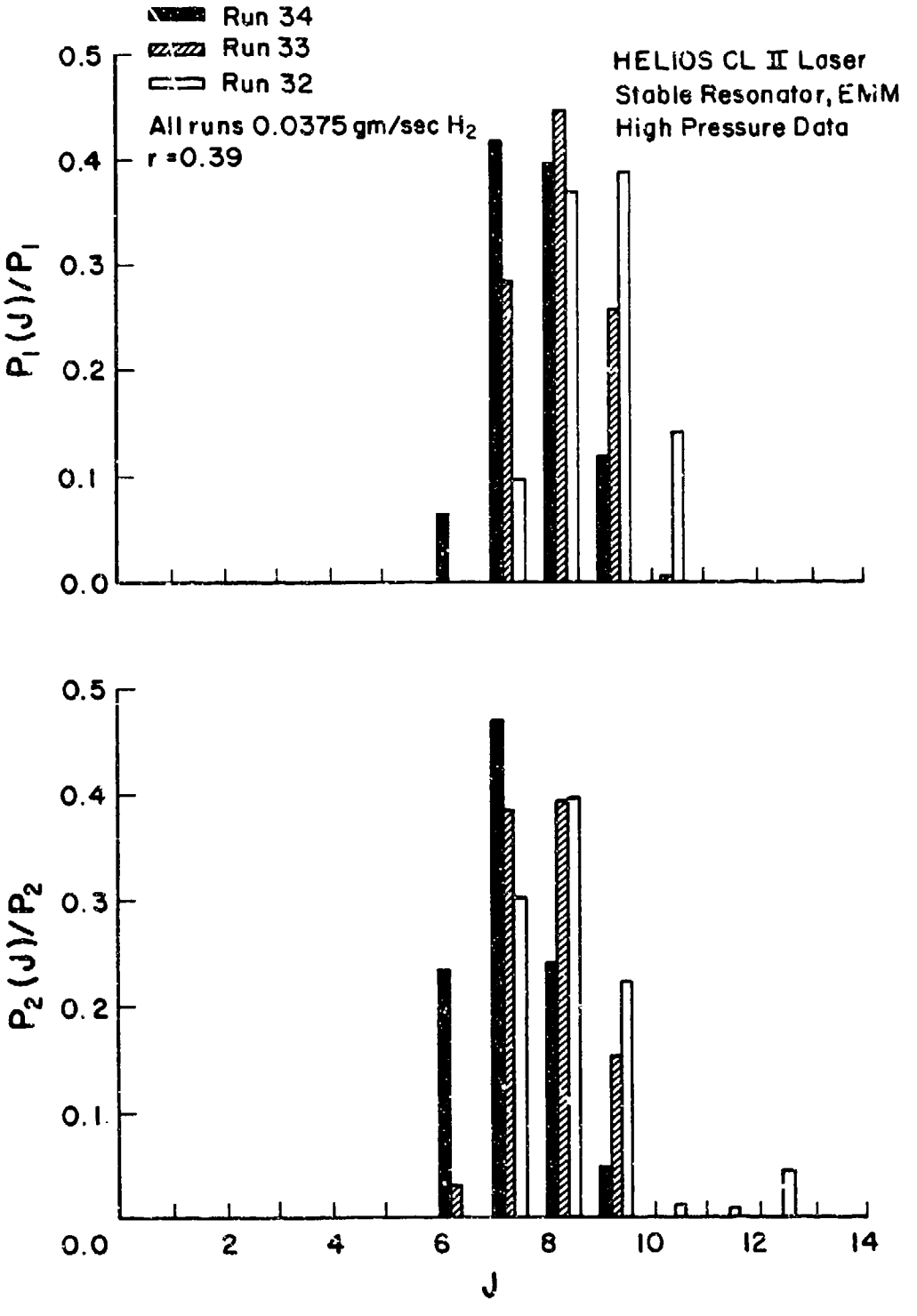

Figure 4. Experimental high pressure stable resonator power spectral distributions for the Helios CL II laser for three different SF_6 flow rates[6,7]. $\dot{m}_{He}$ = 0.078 gm/sec and $\dot{m}_{O_2}$ = 0.28 gm/sec. r = 0.39.

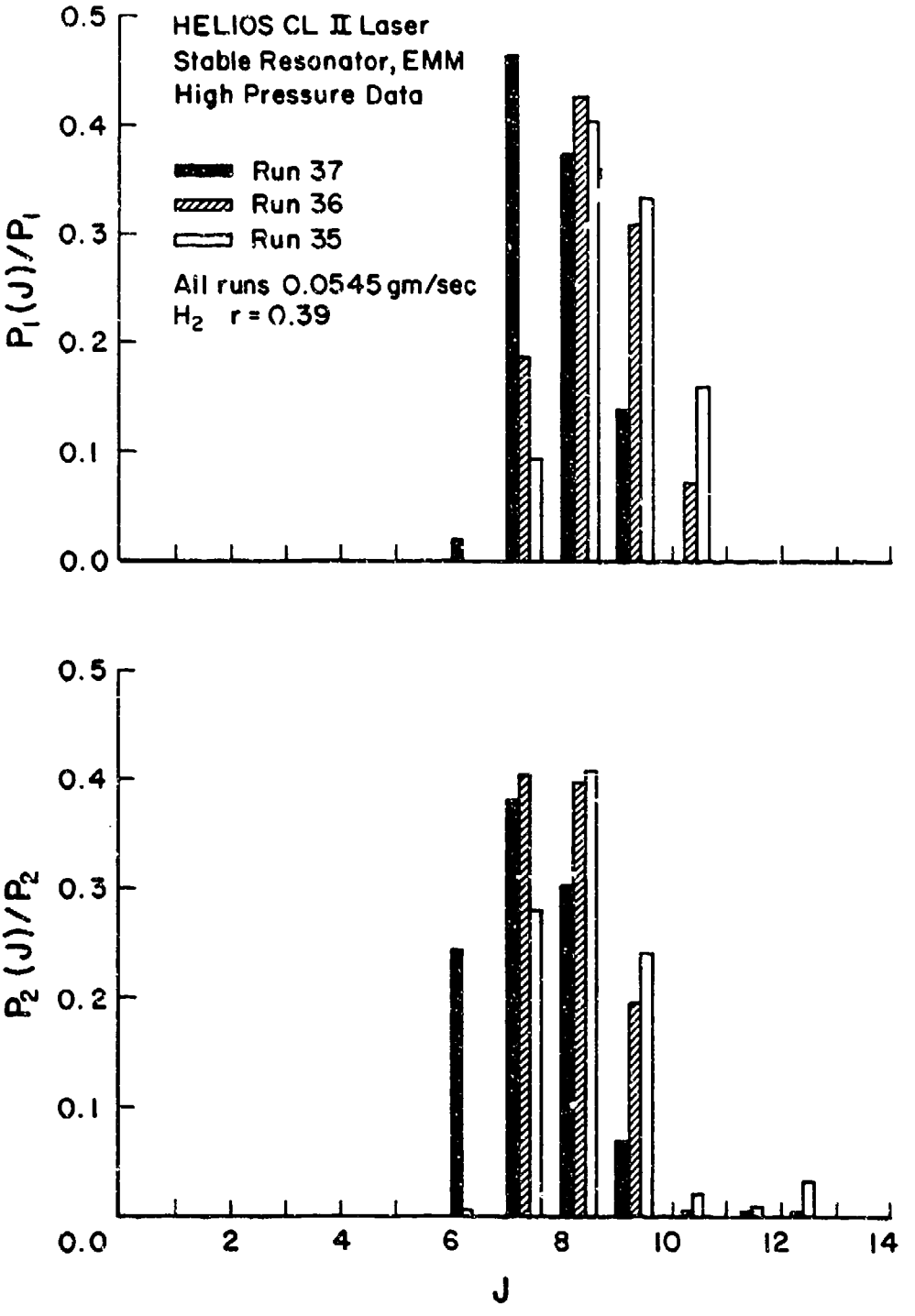

Figure 5. Experimental high pressure stable resonator power spectral distributions for the Helios CL II laser for three different SF_6 flow rates[6,7]. $\dot{m}_{He}$ = 0.078 gm/sec and $\dot{m}_{O_2}$ = 0.28 gm/sec. r = 0.39.

stable resonator data for Runs 33, 34, 36 and 37 in Figs. 6, 7, 8 and 9 respectively. The comparison shows that the MNORO3[9] power spectral distributions are in reasonable agreement with the data. The model predicts the peak of the power spectral distribution either one or two J's too low as it does in the high pressure case[2,3,5,9]. The difference between the MNORO3 predictions and the experimental data is a consequence of the Fabry-Perot resonator employed in the calculations. When the high pressure calculations were repeated with a stable resonator model, MNORO3SR, which includes the upstream-downstream coupling inherent in such a resonator, the low J lines do not lase and the power spectral distribution is in better agreement with the data[3,7]. A stable resonator calculation for the low pressure case would result in a similar shift in the power spectral distribution which would then be in better agreement with the data.

Comparison of the high and low pressure spectra, Figs. 2, 3, 4 and 5, shows that the minimum in the spectra at $P_2(11)$ occurs in the low pressure cases as well as in the high pressure cases. However, the strength of the lines $P_2(10)$ to $P_2(12)$ are weaker in the low pressure cases. This supports the interpretation [6,7] of this minimum as the result of a near resonant energy transfer from v=3, J=3, 4 to v=2, J=14 with a subsequent rotational cascade to v=2, J=11, which is the upper level for the $P_2(12)$ line, which lases, thus blocking the rotational cascade to v=2, J=10, which is the upper level for the $P_2(11)$ line which is thus weaker than the $P_2(12)$ line. Since the HF relaxation rate is proportional to pressure squared, a phenomenon which is based on collisional energy transfer should decrease in magnitude as the pressure decreases, which is shown by the data.

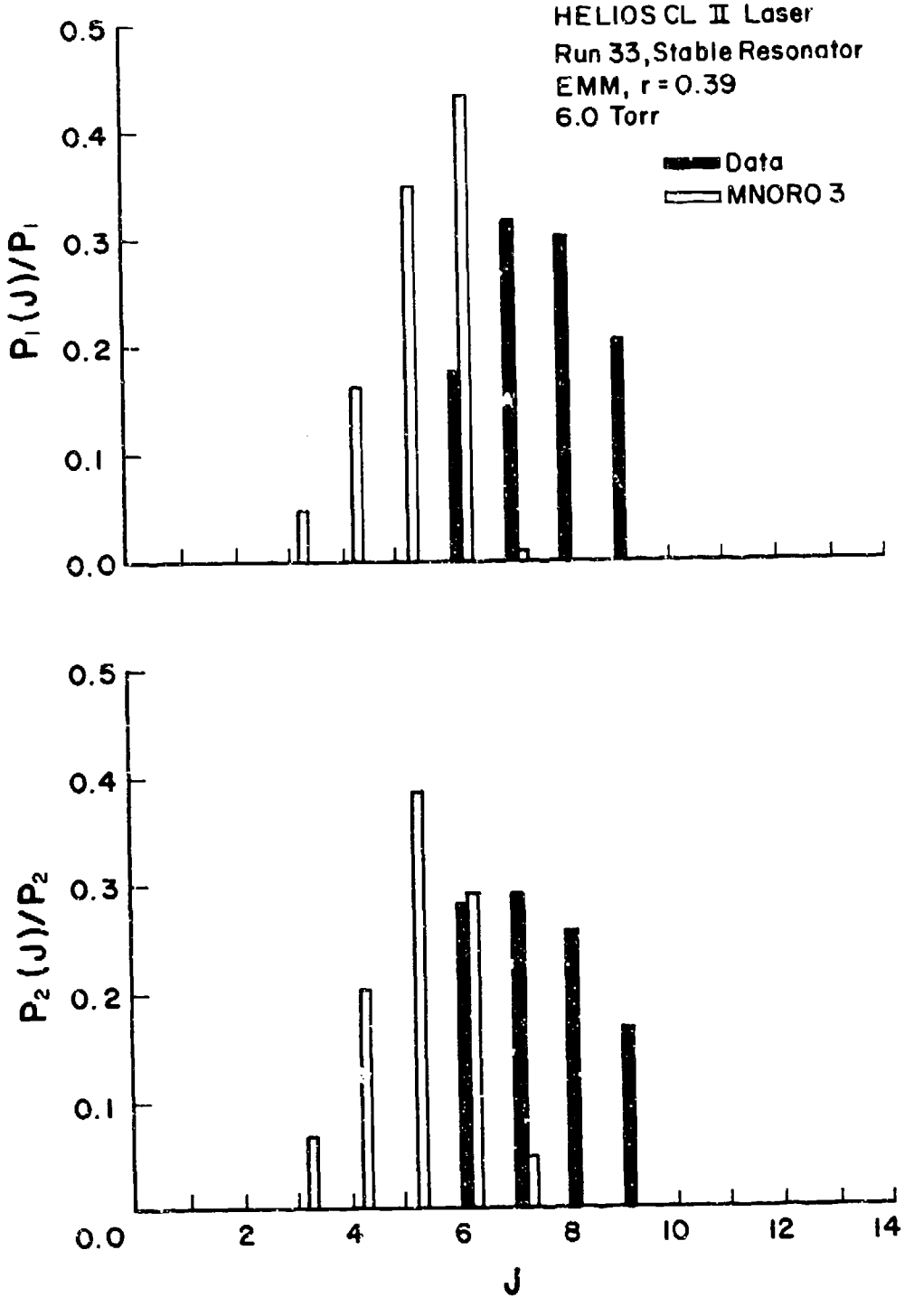

Figure 6. Comparison of the low pressure experimental stable resonator and MNORO3 power spectral distributions for the Helios CL II laser for Run 33 for external mirror mounts, r = 0.39.

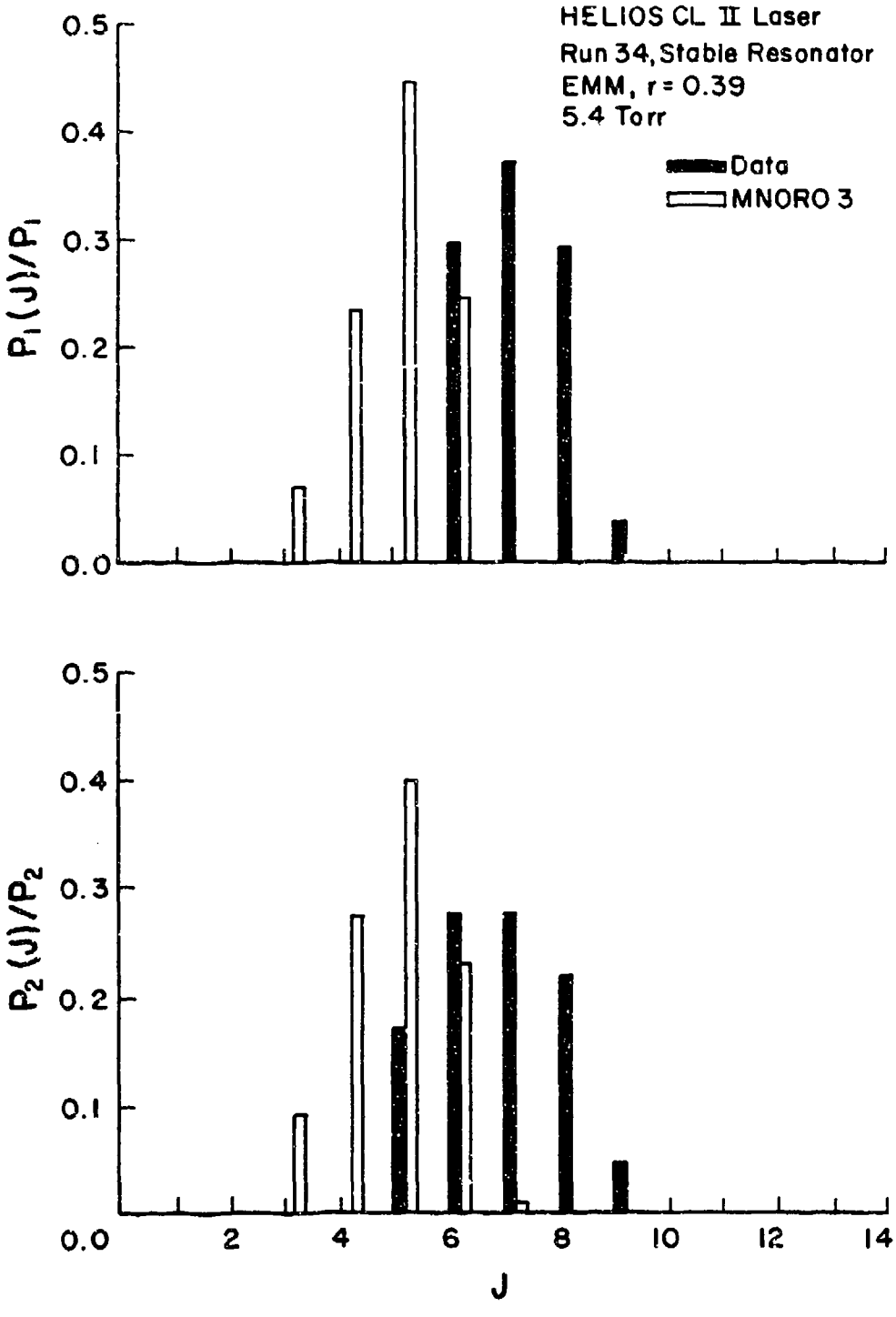

Figure 7. Comparison of the low pressure experimental stable resonator and MNORO3 power spectral distributions for the Helios CL II laser for Run 34 for external mirror mounts, r = 0.39.

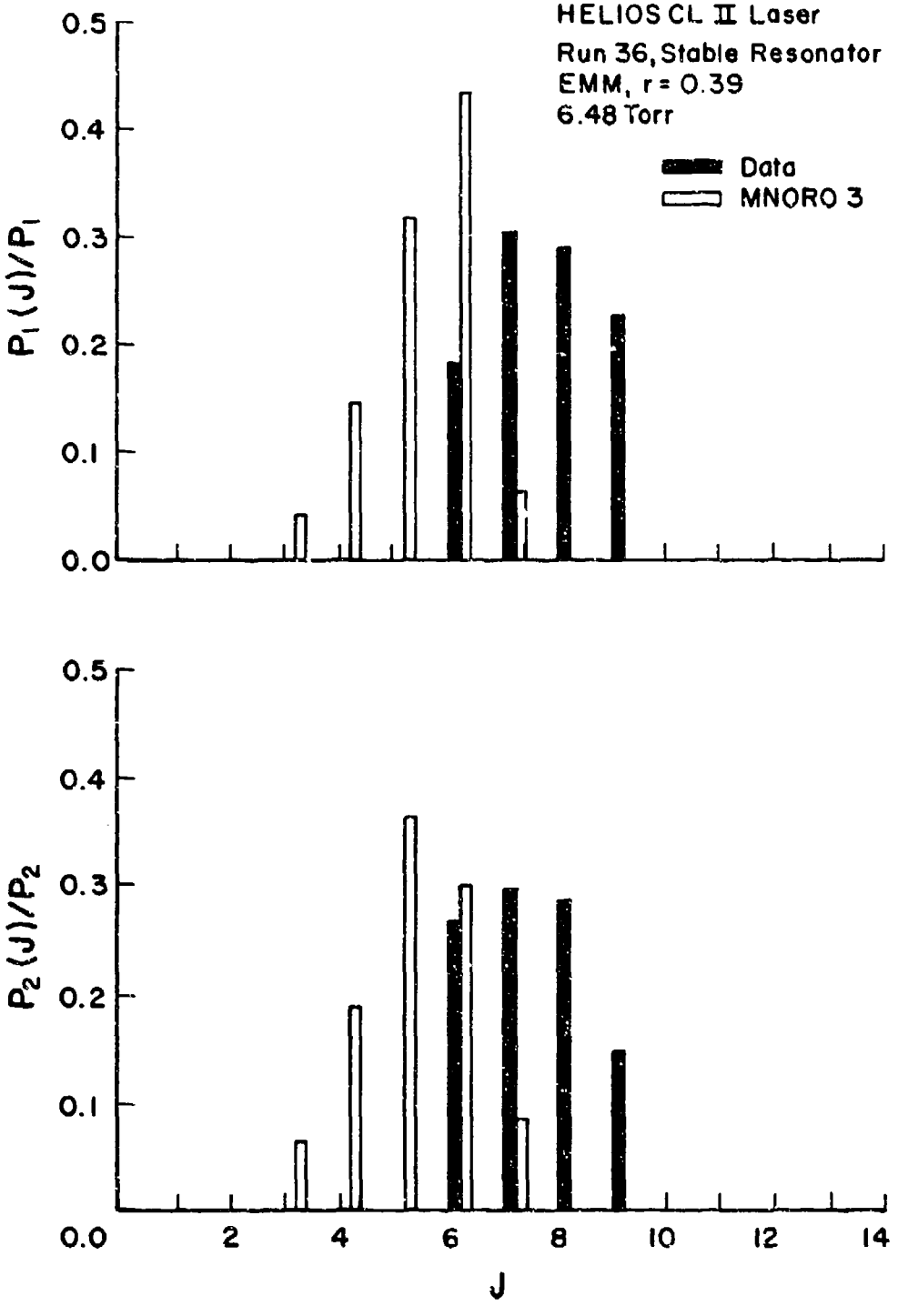

Figure 8. Comparison of the low pressure experimental stable resonator and MNORO3 power spectral distributions for the Helios CL II laser for Run 36 for external mirror mounts, r = 0.39.

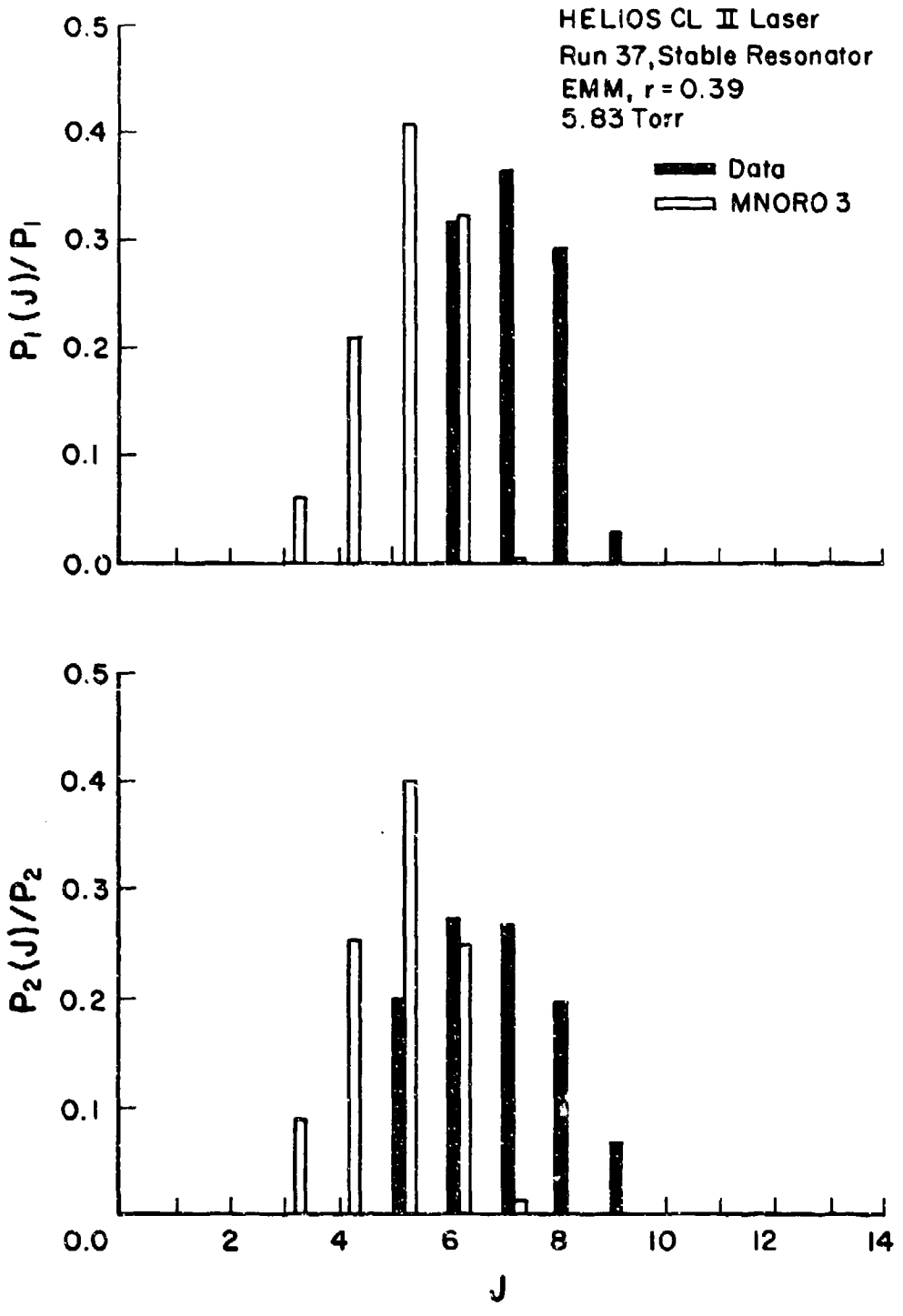

Figure 9. Comparison of the low pressure experimental stable resonator and MNORO3 power spectral distributions for the Helios CL II laser for Run 37 for external mirror mounts, r = 0.39.

The preceding comparisons show that the model agrees with the data as flow rates, cavity losses and pressure are varied. This provides confidence in the model's prediction of the lengths of the saturated gain zones of the lasing lines. Since the low pressure Run 34 gave the largest beam diameter i.e. the longest gain zones, the unstable resonator experiments were performed for this flow rate.

III. TIME-DEPENDENT OSCILLATONS ON LINES WHOSE SATURATED GAIN DOES NOT FILL THE UNSTABLE RESONATOR

The objectives of this study were to measure the frequency and amplitude of the time dependent oscillations in the power spectral output which have been predicted to occur in cw chemical lasers employing unstable resonators to extract power[1,2]. These time dependent fluctuations in cw power, which were shown to be a consequence of rotational nonequilibrium, were shown to occur on lines whose saturated gain zone does not fill the unstable resonator; the amplitude of the fluctuation is determined by the fraction of the resonator filled by the saturated gain zone of the oscillating line, and the frequency of the fluctuation is determined by the geometric outcoupling ratio and the fraction of the resonator that is filled by the saturated gain of the oscillating line[1,2]. The length of the saturated gain zones of the lasing lines was shown to be independent of the size of the resonator[2].

To assist in selecting the flow conditions and resonator geometry to be employed in the experimental measurement of these time-dependent oscillations, a series of calculations with the coupled rotational nonequilibrium-wave optics model, MNORO3UR[3], were performed for the Helios CL II laser for the Run 36 flow rates. These calculations showed that the time-dependent oscillations which may occur on lines whose saturated gain does not fill the resonator are Fresnel number dependent. The time dependent oscillations did not occur for a Fresnel number of 1.5 but did occur for a Fresnel number of 18.57 and for an intermediate Fresnel number of 9.457. For both the large and intermediate Fresnel numbers, the flow conditions had to be altered to stretch the gain zones of the lasing lines. It was shown for the intermediate Fresnel number of 9.457 that,

when the standard flow conditions were used, the gain zones were not long enough for any lines to lase. When the flow conditions were altered, the Fresnel number of 18.57 gave a 10% amplitude variation of the total power and the Fresnel number of 9.457 gave a 15% to 20% amplitude variation of the total power. The intermediate Fresnel number had a larger amplitude variation because the saturated gain filled a smaller fraction of the resonator.

For all cases in which lines oscillated, the period was mostly 6 iterations with some lines varying between 5 and 6 or 6 and 7 iterations[3]. Since the mirror spacing was one meter and each iterate corresponds to one round trip of the radiation through the resonator, the period was mostly 40 ns with some lines varying between 33 and 40 or 40 and 47 ns independent of Fresnel number.

Since the preceding calculations indicated that the experiments should be performed with the longest gain zones possible and the low pressure stable resonator data indicated that this occurred for the flow rates of Run 34, these were the flow rates chosen for the time-dependent experiments. To obtain an a priori estimate of the periods and amplitudes of the time-dependent oscillations for these conditions, the MNORO3UR code was run for the flow rates of Run 34 at 5.4 torr.

3.1 RUN 34 MNORO3UR UNSTABLE RESONATOR CALCULATIONS

Since the low pressure stable resonator results (Chapter II) showed that the low pressure Run 34 flow rates gave the longest gain zones, the MNORO3UR model was run for these flow conditions for a 50% geometric outcoupled, symmetric, confocal, unstable resonator with a 1.0 cm diameter

concave mirror. For completeness, a brief description of this model is given here. The efficient, rotational nonequilibrium, chemical kinetic, fluid dynamic model, denoted MNORO3[9], was coupled to the AFWL physical optics strip resonator model[10]. The resulting code is denoted MNORO3UR. The geometry of the confocal unstable resonator is shown in Fig. 10. The MNORO3 model employed assumes that the flow and the chemistry are independent of the transverse coordinate z. The optical cavity is modeled as a strip, confocal unstable resonator. The beam is diffractively propagated through the cavity using a solution of the Huygens-Fresnel integral which is obtained by a fast Fourier transform technique. The optics model is coupled with the kinetics model through the thin skin gain approximation in which the active medium is assumed to be a thin sheet in front of the large mirror. The solution is an iterative one. The calculation starts by passing a plane wave of roughly the expected intensity through the empty cavity. The resulting intensity distribution is sent to the chemistry. The species equations are solved with the given intensity distribution, and the thickness of the mixed flow, L_e, and the gains on each line are calculated and sent to the optics. The stored wave from the preceding optics calculation is then propagated through the cavity and incremented by the gain distribution from the chemistry. This process is repeated until the difference between successive iterates is less than some prescribed amount.

Because each iterate in the solution of the steady state equations corresponds to one round trip of the radiation through the cavity, each iterate may be regarded as a time step in the development of the steady-state solution[1]. The steady-state iterates are related to the solution of

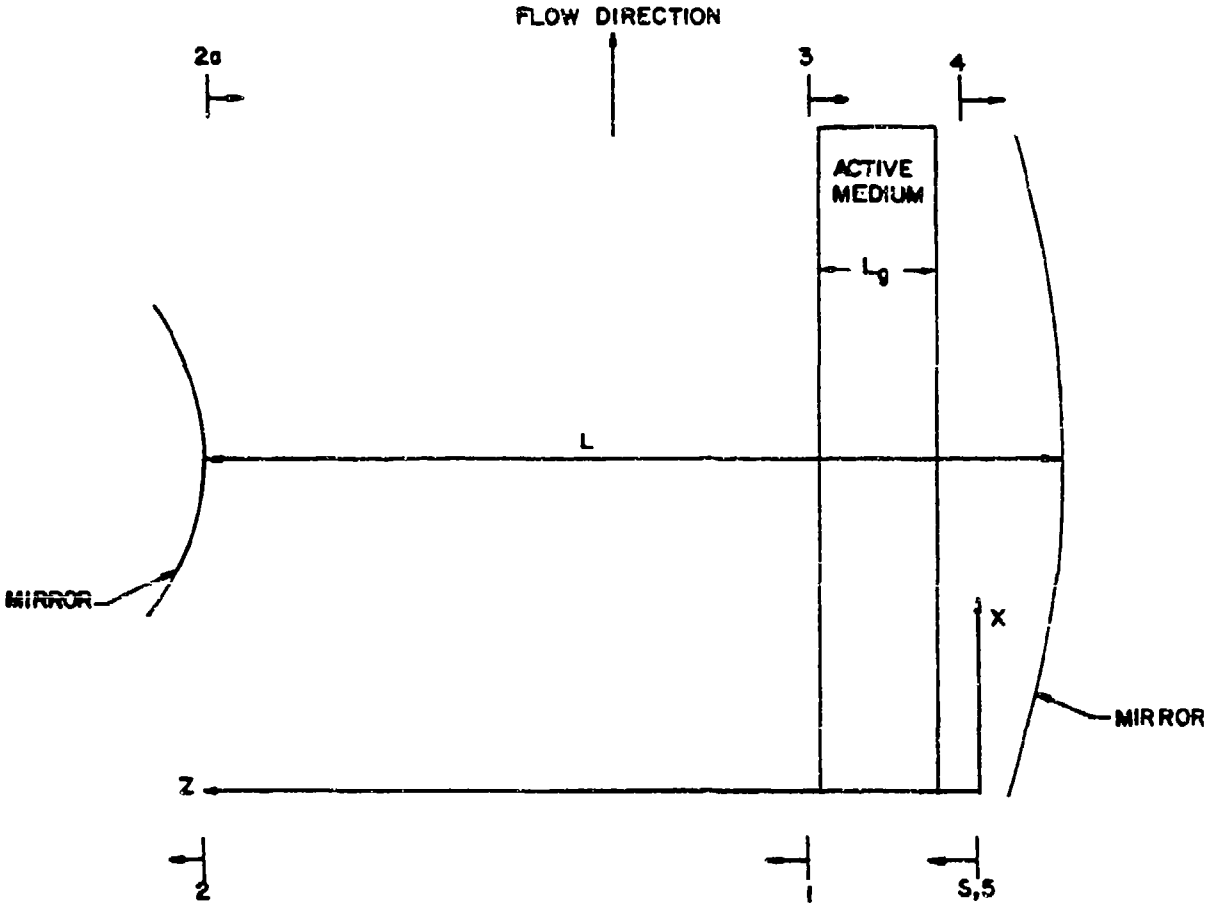

Figure 10. Confocal unstable resonator geometry and schematic of the wave propagation through the resonator.

the time-dependent equations in the following way. The equations governing the time-dependent problem are of the form

$$\rho\left[\frac{\partial n}{\partial t} + u\,\frac{\partial n}{\partial x}\right] = \chi_{chem} + \chi_{rad} \tag{3.1-1}$$

for the populations of the lasing species and

$$\frac{1}{c}\,\frac{\partial I^{\pm}}{\partial t} + \frac{\partial I^{\pm}}{\partial z} = \alpha(I^{\pm} + s) \tag{3.1-2}$$

assuming the radiation travels in the z direction only. To construct the solution of these equations, they are written in the form

$$\frac{\partial n}{\partial t} = -\,u\,\frac{\partial n}{\partial x} + \frac{1}{\rho}\,\chi_{chem} + \frac{1}{\rho}\,\chi_{rad} = f(t) \tag{3.1-3}$$

$$\frac{1}{c}\,\frac{\partial I^{\pm}}{\partial t} = -\,\frac{\partial I^{\pm}}{\partial z} + \alpha(I^{\pm} + s) = h(t) \tag{3.1-4}$$

These equations are discretized in the space variables to convert them into ordinary differential equations in time. The solution at time $t + \Delta t$ is of the form

$$n(t + \Delta t) = n(t) + f(t)\,\Delta t \tag{3.1-5}$$

$$I(t + \Delta t) = I(t) + ch(t)\,\Delta t \tag{3.1-6}$$

To obtain only the steady state solution, the time derivatives in Eqs. (3.1-3) and (3.1-4) are set to zero which gives

$$0 = -\,u\,\frac{\partial n}{\partial x} + \frac{1}{\rho}\,\chi_{chem} + \frac{1}{\rho}\,\chi_{rad} \tag{3.1-7}$$

$$0 = -\frac{\partial I^{\pm}}{\partial z} + \alpha(I^{\pm} + s) \tag{3.1-8}$$

To obtain the steady-state solution, Eq. (3.1-8) is solved for $I^{\pm}(x)$ which is then substituted into Eq. (3.1-7). Eq. (3.1-7) is then solved for $\alpha(x)$ which is then substituted into Eq. (3.1-8) and the process is repeated. When the iteration procedure has converged, $I(x)$ and $\alpha(x)$ remain the same for successive iterates.

Prior to convergence, when $I_{n-1}(x)$ and $\alpha_{n-1}(x)$ are substituted into Eqs. (3.1-7) and (3.1-8), they sum to a non-zero value which would be equal to the corresponding time derivative in the time-dependent equations, i.e.,

$$\frac{\partial n}{\partial t} = \delta \tag{3.1-9}$$

$$\frac{1}{c}\frac{\partial I^{\pm}}{\partial t} = \delta' \tag{3.1-10}$$

This would give solutions for $I(t)$ and $n(t)$ of the form

$$n(t) = n_o + \delta\,\Delta t \tag{3.1-11}$$

$$I(t) = I_o + c\delta'\Delta t \tag{3.1-12}$$

for small Δt (1 round trip through the resonator in this case). Comparison of Eqs. (3.1-11) and (3.1-12) with Eqs. (3.1-5) and (3.1-6) shows that they have the same form. Thus, each iterate in the steady-state solution procedure corresponds to a time step in the development of the time

dependent solution.

For the case of the radiative transfer equation treatment of the radiation part of the problem, the equivalence between the steady-state solution obtained from the iterative solution of the steady-state equations and the steady-state solution obtained from the solution of the time-dependent equations as t goes to infinity was shown by Schimke[11]. Based on this result, the use of Eqs. (3.1-9) and (3.1-10) to modify the $I_{n-1}(x)$ and $\alpha_{n-1}(x)$ before calculating the next iterate of the steady-state equations might speed up the rate of convergence of the iteration procedure.

Total power, Fig. 11, and the power on individual lines, Fig. 12, as calculated by MNORO3UR, are plotted versus iteration number. Because each iterate corresponds to one round trip of the radiation through the cavity, each iterate may be regarded as a time step in the development of the steady-state solution as described above. Thus, fluctuations in the power from iterate to iterate may be regarded as time-dependent oscillations. Since the spacing between the convex and concave mirrors was 100 cm, the round trip transit time was 6.67 ns. Thus, the period of an oscillation is calculated by multiplying the number of iterates for one period by 6.67 ns. The frequency of the oscillation is the inverse of the period. The percent amplitude modulation was calculated by dividing the peak to peak power difference by the average power. Table 3 is a summary of the period, frequency, percent amplitude modulation, and power for the total beam and for the individual lines shown in Figs. 11 and 12. From this table, it is seen that the characteristics of the Run 34 oscillations are the same as those predicted for Run 36. Thus, experimentally the oscillations are

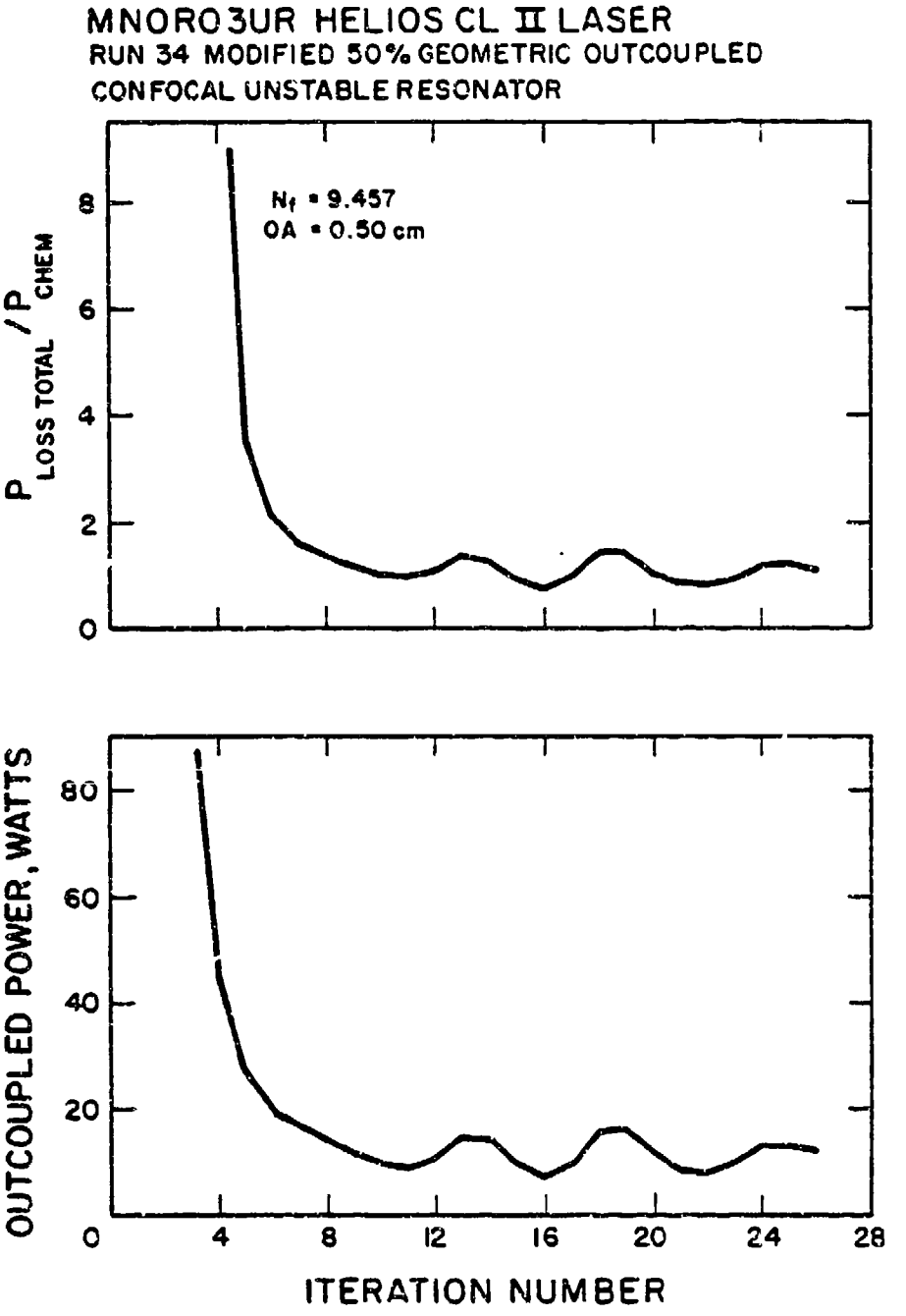

Figure 11. MNORO3UR convergence parameter $P_{loss\ total}/P_{chem}$ and the multiline outcoupled power calculated in the optics[3], P_{out}, versus iteration number for rotational nonequilibrium for a 50% geometric outcoupled, confocal, unstable strip resonator with a large mirror diameter of 1.0 cm for the Helios CL II laser for Run 34 at 5.4 torr.

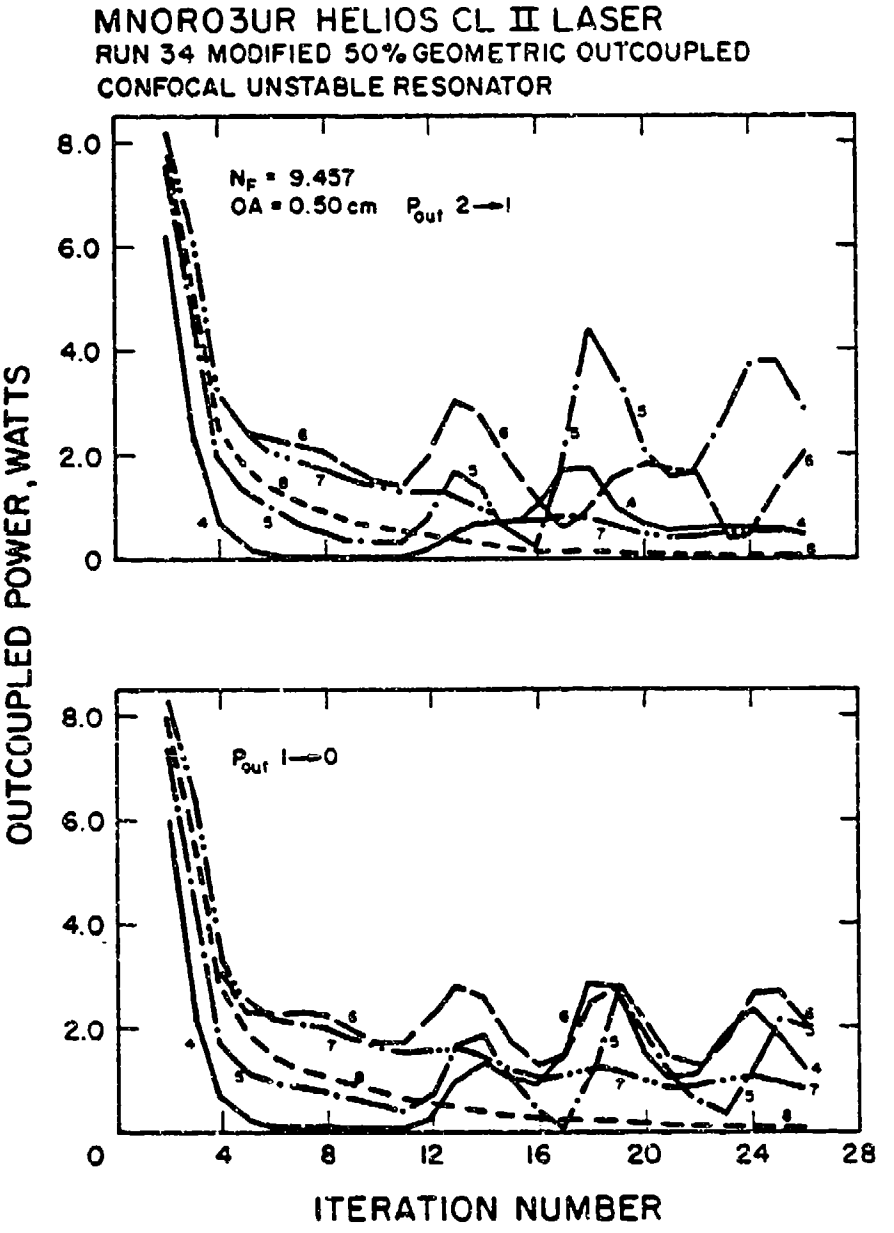

Figure 12. MNOR03UR outcoupled power [3], P_{out}, for individual lines versus iteration number for a 50% geometric outcoupled, confocal, unstable strip resonator with a large mirror diameter of 1.0 cm for the Helios CL II laser for Run 34 at 5.4 torr.

Line	Period	Frequency	Amplitude Modulation	Power
	ns	MHz	% P_V (J)	Watts
Total Power	40	25	64*	11.00
$P_1(4)$	33	30	41	1.70
$P_1(5)$	40	25	75	1.20
$P_1(6)$	40	25	37	1.90
$P_1(7)$	33	30	30	1.00
$P_1(8)$				0.05
$P_2(4)$	40	25	50	0.60
$P_2(5)$	33	30	81	2.70
$P_2(6)$	40-47	21-25	64	1.10
$P_2(7)$	33-40	25-30	40	0.50
$P_2(8)$				0.05

*Amplitude Modulation for Total Power: % P_T

Table 3. MNORO3UR time-dependent oscillation periods, frequencies, and amplitude modulations (% $P_V(J)$) for a 50% geometric outcoupled confocal unstable resonator with a 5 mm slit at RUN 34 flow rates with a 5.4 torr cavity pressure.

expected to exhibit a period of about 40 ns with their amplitude modulation increasing as the fraction of the resonator filled by the saturated gain decreases. In the next section, the unstable resonator used in the time-dependent experiments and the procedure used to align it are described.

3.2 CONFOCAL UNSTABLE RESONATOR ALIGNMENT PROCEDURE

Figure 13 shows the layout of the 50% geometric outcoupled, confocal, unstable resonator used on the Helios CL II laser. The resonator consists of a convex and a concave mirror separated by 100 cm, with a flat scraper mirror placed at an angle of 45° to the optical axis near the convex mirror. The radius of curvature of the mirrors is -200 cm for the convex mirror and 400 cm for the concave mirror which result in a resonator magnification of 2. The scraper mirror consists of two flat mirrors which slide apart to form a slit whose width could be varied from 0.0 to 1.0 cm. Since the resonator was a confocal, unstable resonator with a magnification of 2, the effective diameter of the convex mirror is equal to the scraper mirror slit width and the effective diameter of the concave mirror is equal to twice the scraper mirror slit width. The Fresnel number for the resonator is determined by the effective diameter of the concave mirror[12] and is therefore controlled by the slit width of the scraper mirror. The Fresnel number for the resonator used on the Helios CL II laser ranged from 0.0 to 35.7.

Figure 14 shows the optical path of the alignment HeNe laser through the unstable resonator. The resonator's mirrors were mounted on a set of translation stages which permitted accurate positioning of the optical axis

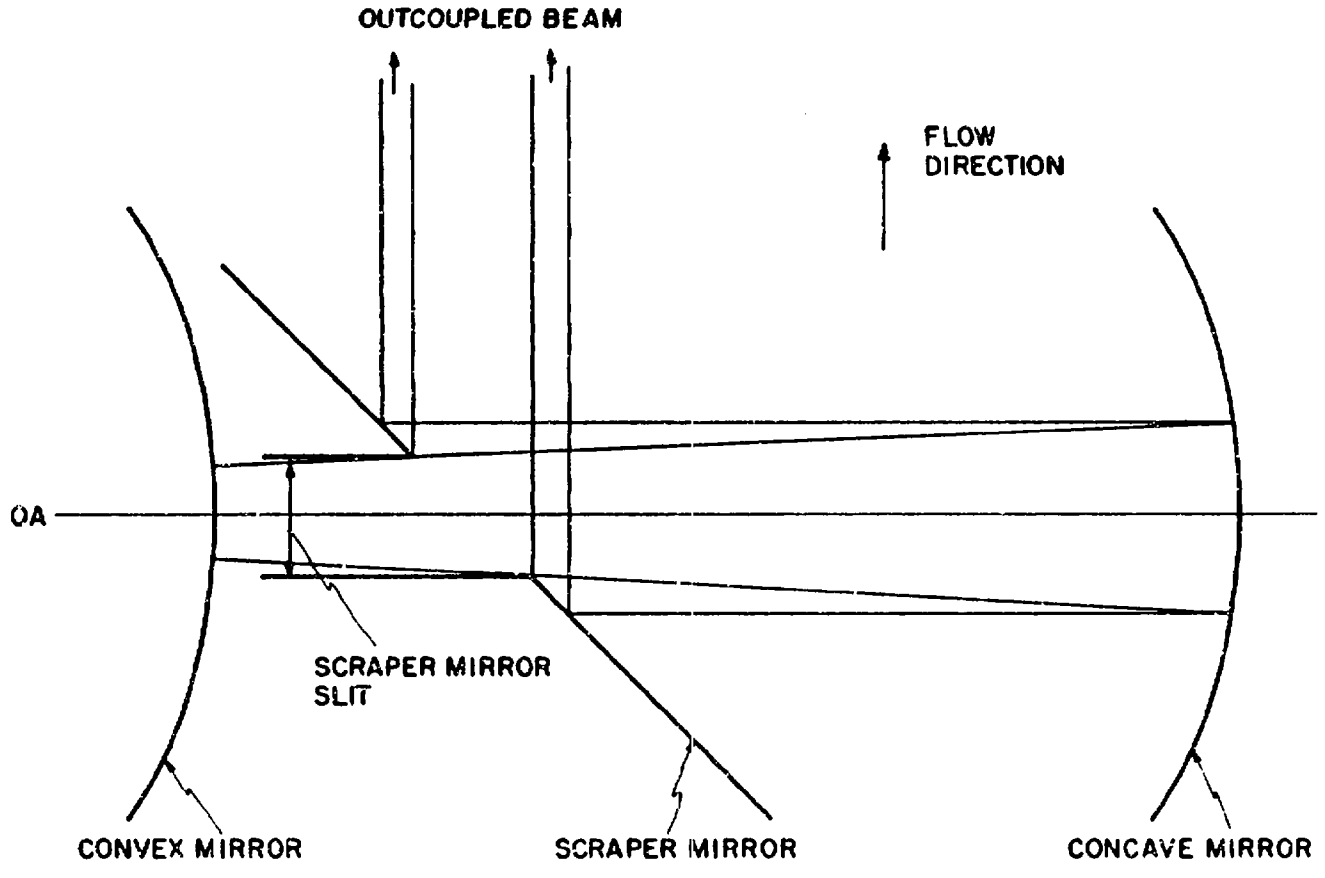

Figure 13. Layout of the unstable resonator used in the measurement of the time-dependent oscillations on lines whose saturated gain does not fill the resonator.

OPTICAL PATH OF THE HeNe ALIGNMENT LASER THROUGH THE CONFOCAL UNSTABLE RESONATOR

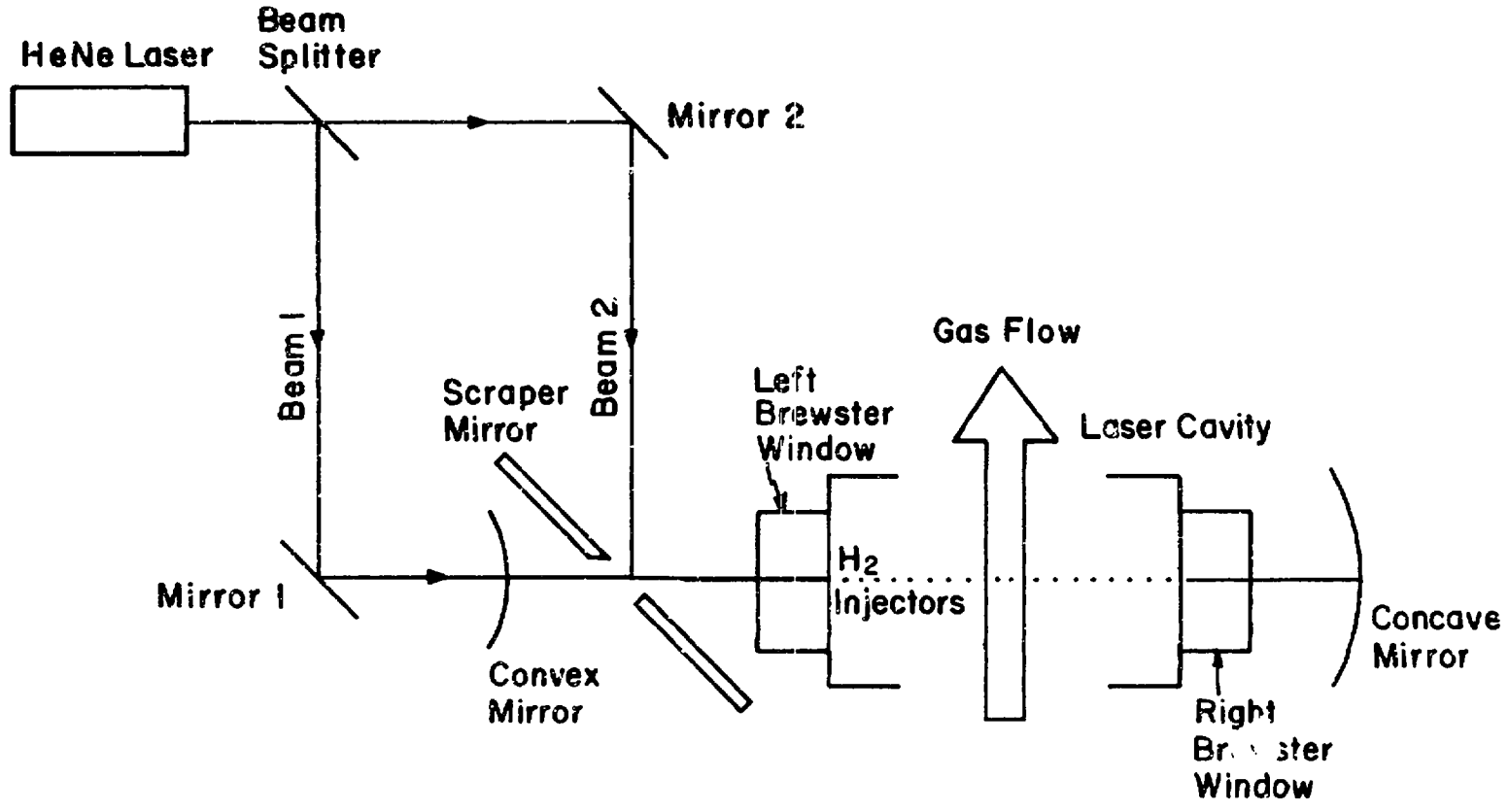

Figure 14. Optical path of the HeNe alignment laser through the confocal, unstable resonator.

of the resonator with respect to the H_2 injectors. The unstable resonator alignment procedure consisted of five steps.

The first step aligned the HeNe laser beam with the H_2 injectors of the laser. The Brewster windows and the resonator mirrors were removed from their mounts for this step of the alignment procedure. The HeNe laser was set at a height equal to the height of the center of the laser cavity plus the necessary additional height to compensate for the refraction offset due to the left Brewster window when it is in place. An iris mounted on a magnetic base, which was set to the HeNe beam height, was used to check that the HeNe beam was at the proper height during the alignment procedure. The HeNe beam was split into two components as shown in Fig. 14. Mirror 1 was adjusted until beam 1 was aligned with the H_2 injectors in the laser cavity. The left Brewster window was then attached to the laser. Fine adjustments were made to mirror 1 until the beam exited the right side of the laser cavity, centered vertically and parallel to the H_2 injectors. The right Brewster window was then attached to the laser. The height of the HeNe beam was checked with the iris at the far right of the laser. If necessary, mirror 1 was again adjusted to correct any error in the alignment of the HeNe beam with respect to the laser cavity.

The second step in the alignment procedure was to center the mirror holders on the HeNe beam. The translation stages are located on the optical table so that their range of travel permits movement of the optical axis upstream as well as downstream of the H_2 injectors. The alignment of the mirror holders on the translation stages was achieved by using a set of plexiglass disks which fit into the mirror mounts. Each disk had a small hole the diameter of the HeNe beam drilled in its center. The mounts were

adjusted on the translation stages until the alignment beam passed through each hole.

The next step in the alignment procedure was the placement of the concave mirror. The concave mirror was placed in its mount and tuned until beam 1 reflected back on itself.

The fourth step was the alignment of the scraper mirror. There are two types of scraper mirrors that were used. One consists of two plane mirrors in an adjustable mount which allowed the vertical slit between them to be varied from 0 to 1 cm. The other was a plane, silver coated, copper mirror 1.75 inches in diameter with a rectangular hole 1.5 mm in the vertical direction and 7.07 mm in the horizontal direction, which corresponds to an effective width of 5.0 mm in the flow direction. The planes of both mirrors were placed at 45° to the optical axis of the resonator. The alignment procedure depends upon the scraper mirror used.

The variable slit scraper mirror was placed in its mount and the slit fully opened. The position of each half of the variable slit mirror is controlled by a micrometer. Each side in turn was moved in until it blocked out beam 1 and the micrometer reading was recorded. The micrometers were then both set shorter than the previous readings by half the diameter of the HeNe beam. The mirror halves would just touch at this setting. Then each mirror was moved back half a beam diameter. The HeNe image reflected back by the concave mirror would then appear symmetric about the scraper mirror slit. Mirror 2 was then adjusted until beam 2 was centered on the slit and the image of beam 1 from the scraper mirror was symmetric about beam 2 on mirror 2 and on the face of the HeNe laser.

The rectangular hole scraper mirror alignment procedure was as

follows. The rectangular hole scraper mirror was positioned in its holder by eye until the HeNe image reflected from the concave mirror was centered in the rectangular hole. Mirror 2 was then adjusted until beam 2 was centered in the rectangular hole and the image of beam 1 from the scraper mirror appeared symmetric about beam 2 on mirror 2 and on the face of the HeNe laser.

The last step was the alignment of the convex mirror. The convex mirror was placed in its mount, which blocked beam 1. By adjusting the convex mirror, beam 2 is made to reflect back upon itself through the resonator and back to the HeNe laser. When the variable slit scraper mirror was used, the slit size was reduced to obtain a smaller reference spot which resulted in a more accurate alignment of the convex mirror.

It should be noted that beam 2 then represents the path of the IR output beam when the Helios CL II laser is run.

3.3 EXPERIMENTAL PROCEDURE

Figure 15 is a schematic of the experimental set up to measure the frequency and amplitude of the time-dependent oscillations on lines whose saturated gain does not fill the resonator. A room temperature InAs fast detector (~ 2 ns rise time) was used to measure the oscillations. The detector consisted of a 0.25 mm square InAs photodiode in a TO-18 package, Judson Infrared model J-12LD. The circuit for the InAs detector is shown in Fig. 16. Total beam oscillations were measured by passing the output beam through a mechanical chopper and then into the InAs detector, Fig. 15. Oscillations on individual lines were measured by passing the output beam through a constant efficiency spectrometer[13] and a mechanical chopper,

SCHEMATIC OF THE EXPERIMENT TO MEASURE THE TIME - DEPENDENT OSCILLATIONS ON LINES WHOSE SATURATED GAIN DOES NOT FILL THE RESONATOR

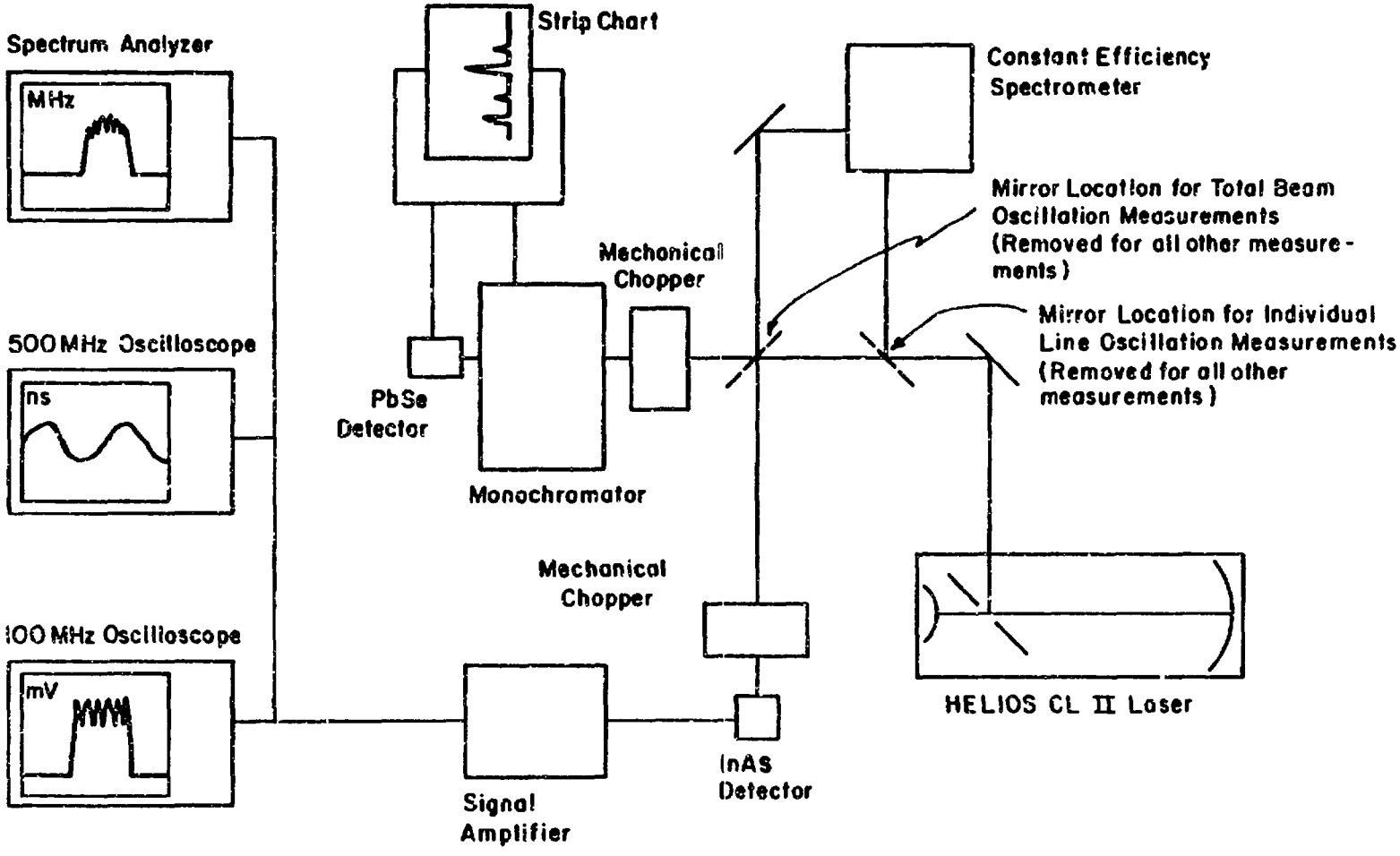

Figure 15. Schematic of the experiment to measure the time-dependent oscillations on lines whose saturated gain does not fill the unstable resonator.

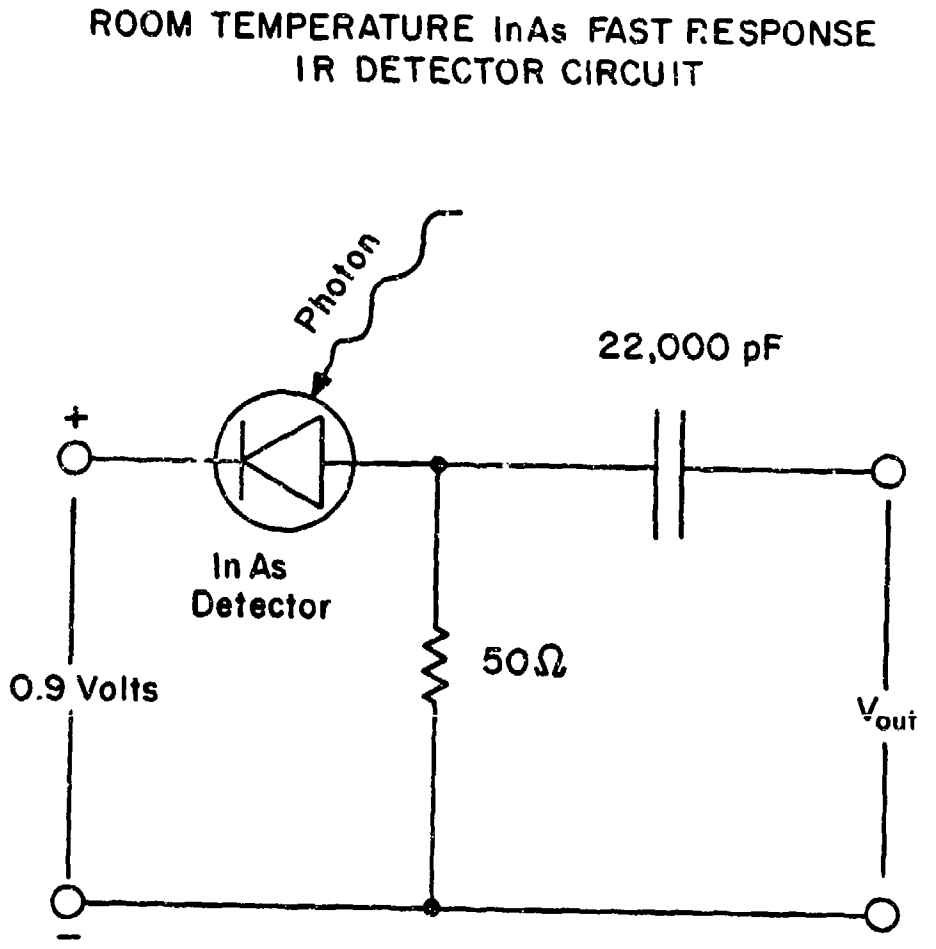

Figure 16. Electrical circuit for the room temperature InAs fast response detector. The detector consists of a Judson J12LD diode, 50 ohm resistor and a 22,000 pf capacitor. The response time is ~ 2 ns.

which allowed the output of one line at a time to impinge on the detector. To obtain the period of the oscillation, the output from the detector was amplified and displayed on a 500 MHz oscilloscope. To determine the frequency spread of the oscillations, the signal was also displayed on a 40 MHz spectrum analyzer. Since the 500 MHz oscilloscope could only display the AC part of the signal, to obtain the amplitude modulation, the signal was displayed on a 100 MHz oscilloscope. Power spectral distributions were taken by passing the output through a mechanical chopper, a monochromator and into a room temperature PbSe detector. The PbSe detector and the monochromator were both connected to a strip chart to record the relative powers of the lasing lines.

3.4 RUN 34, LOW PRESSURE, SLIT SCRAPER MIRROR DATA

Oscillation frequency and amplitude measurements for the low SF_6 and low H_2 flow rates, Run 34, were taken with the flow control valve wide open, which gave a laser cavity pressure of 5.3 torr. In Chapter II it was shown that this flow condition produced the longest saturated gain zones for the Helios CL II laser. Because the resonator was symmetric, the distance between the optical axis and the H_2 injectors was always equal to the scraper mirror slit width used. Table 4 is a summary of the oscillation data for the total power as a function of Fresnel number. The MNORO3UR calculations for Run 36[3] and Run 34 performed prior to the experiments indicated that the period of the oscillations should be 40 ns independent of Fresnel number. From Table 4, it is seen that in addition to the expected 40 ns oscillation, there was a 7 ns oscillation superimposed on top of it. Since the mirror spacing of the resonator was

Run 34 50% Geometric Outcoupled,
Symmetric, Confocal, Unstable Resonator

Scraper Mirror Slit, mm	N_F	P_{cav} Torr	P_T Watts	OSC Period ns	Amplitude Modulation $\%P_T$
1.0	0.357	5.31	5.25	7	
2.0	1.428	5.30	5.15	7	
3.0	3.214	5.29	4.10	40/7	3.0
4.0	5.714	5.31	1.90	40/7	22.0
5.0	8.929	5.34	0.70	40/7	25.0
6.0	12.857	5.31	0.13	40	50.0

Table 4. Frequency and amplitude of the time-dependent oscillation of total power as a function of Fresnel number for the flow rates of Run 34 at 5.3 torr. The He bottle was running out when the 2 mm through 6 mm data were taken. This caused the total power to be less than that measured when the individual line oscillation data were taken.

100 cm and the round trip transit time is 6.67 ns, the 7 ns oscillation probably corresponds to a mode beating of the laser. Table 4 shows that the time-dependent oscillations on lines whose saturated gain did not fill the resonator did not occur for Fresnel numbers below 1.5. Since the calculations showed that the length of the saturated gain region is independent of the size of the resonator[2], Table 4 shows that the amplitudes increased as the fraction of the resonator filled by the oscillating lines decreased. Fig. 17 shows the total power 100 MHz oscillocope traces for the 4 mm and 2 mm slit widths. Comparison of these traces clearly shows the difference in the traces when the time-dependent oscillations occur.

Table 5 gives the oscillation data for individual lines as a function of Fresnel number. This data shows that the 40 ns time-dependent oscillations on lines whose saturated gain did not fill the resonator did not occur for Fresnel numbers below 1.5. It should be noted that there is a strong cascade coupling between the oscillating 1→0 and 2→1 lines, that is, if $P_2(6)$ oscillates then $P_1(7)$ also oscillates. From a comparison of the 3 mm and 4 mm slit cases, it is generally seen that as the fraction of the resonator filled by a line decreased, the amplitude of its oscillation increased. Figs. 18, 19 and 20 are typical oscilloscope and spectrum analyzer traces of oscillating lines. The 7 ns oscillation superimposed on the 40 ns oscillation is clearly evident in these figures. Comparison of the frequency ranges for the 3 mm and 4 mm slit widths indicates that the frequency is independent of the Fresnel number. Comparison of the traces in Figs. 19 and 20 shows that both $P_1(7)$ and $P_1(8)$ had approximately the same % amplitude modulation, but $P_1(7)$ had nearly five times the power of

Total Power Traces

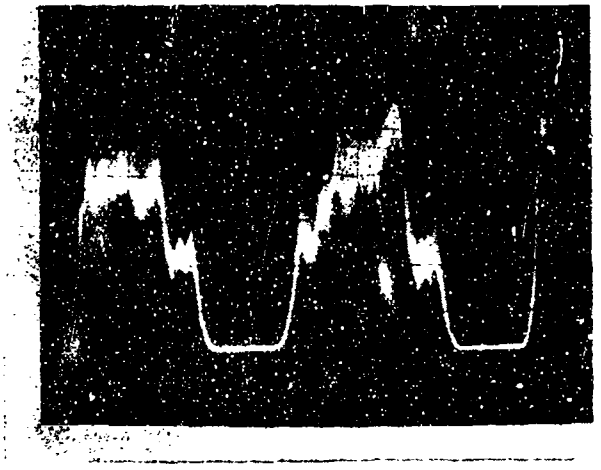

a) 4 mm slit width; all lasing lines oscillating with 40 ns period

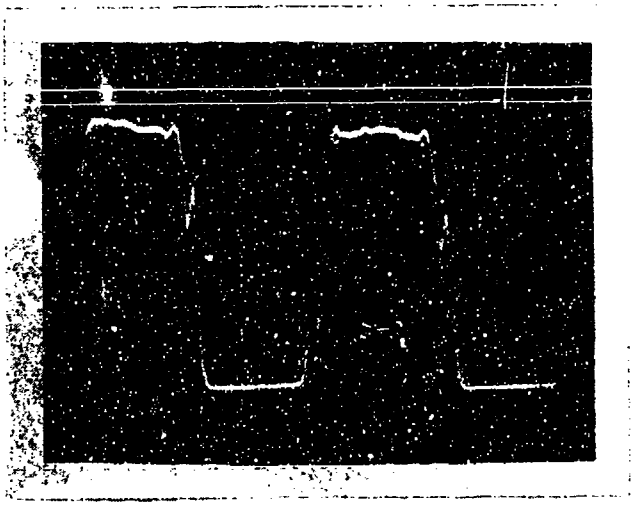

b) 2 mm slit width; no lines oscillating with 40 ns period; some lines exhibited 7 ns oscillation

Figure 17. Typical total power 100 MHz oscilloscope traces for Run 34 flow rates at 5.3 torr showing the difference between the oscilloscope traces of an oscillating and nonoscillating case. For both traces, the scales are 20 mV/division vertically and 0.2 ms/div horizontally.

Run 34 50% Geometric Outcoupled, Symmetric, Confocal, Unstable Resonator
Cavity Pressure 5.3 torr

Scraper Mirror Slit, mm	N_F	Lasing Line	$P_1(4)$	$P_1(5)$	$P_1(6)$	$P_1(7)$	$P_1(8)$	$P_1(9)$	$P_2(5)$	$P_2(6)$	$P_2(7)$	$P_2(8)$	P_T Watts
1.0	0.357	OSC Period, ns	-	-	-				7	7			4.5*
1.5	0.804	OSC Period, ns	-	-	7	-			7	7	-	-	6.4
2.0	1.428	OSC Period, ns (Strength of 7 ns OSC)	-	-	7	7	-		7 (weak)	7	7 (weak)	-	5.9-6.0
		Amplitude Modulation % $P_v(J)$			9	11				13			
3.0	3.214	OSC Period, ns (Strength of 40ns OSC)			40/7 (weak)	40/7	40/7 (weak)	7		40/7	40/7 (weak)	7	4.8-5.1
		OSC Freq., MHz			23-26	23-34	23-30			18-29	25-31		
		Amplitude Modulation % $P_v(J)$				12.5				20-50	12	12.5	
4.0	5.714	OSC Period, ns (Strength of 40ns OSC)			-	40/7	40/7	40 (weak)		40	40/7	40/7	3.5-3.6
		OSC Freq., MHz				20-30	20-30	20-30		20-28	18-30	22-30	
		Amplitude Modulation % $P_v(J)$				38	80			20-30	66	55	

- means the line lased but was too weak to operate the fast detector.
*The H_2 and He bottles were running out when these data were taken. This caused the total power to be less than that measured when the total power oscillation data were taken.

Table 5. Frequency and amplitude of the time-dependent oscillations on individual lines for the flow rates of Run 34 at 5.3 torr as a function of Fresnel number. Individual line data were not obtained for the 5 mm and 6 mm slit widths because the individual lines in these cases were too weak to operate the fast detector. A PbSe detector was used to measure time averaged power spectral distributions. Lines too weak to operate the fast InAs detector would operate the PbSe detector.

Run 34
$P_2(7)$

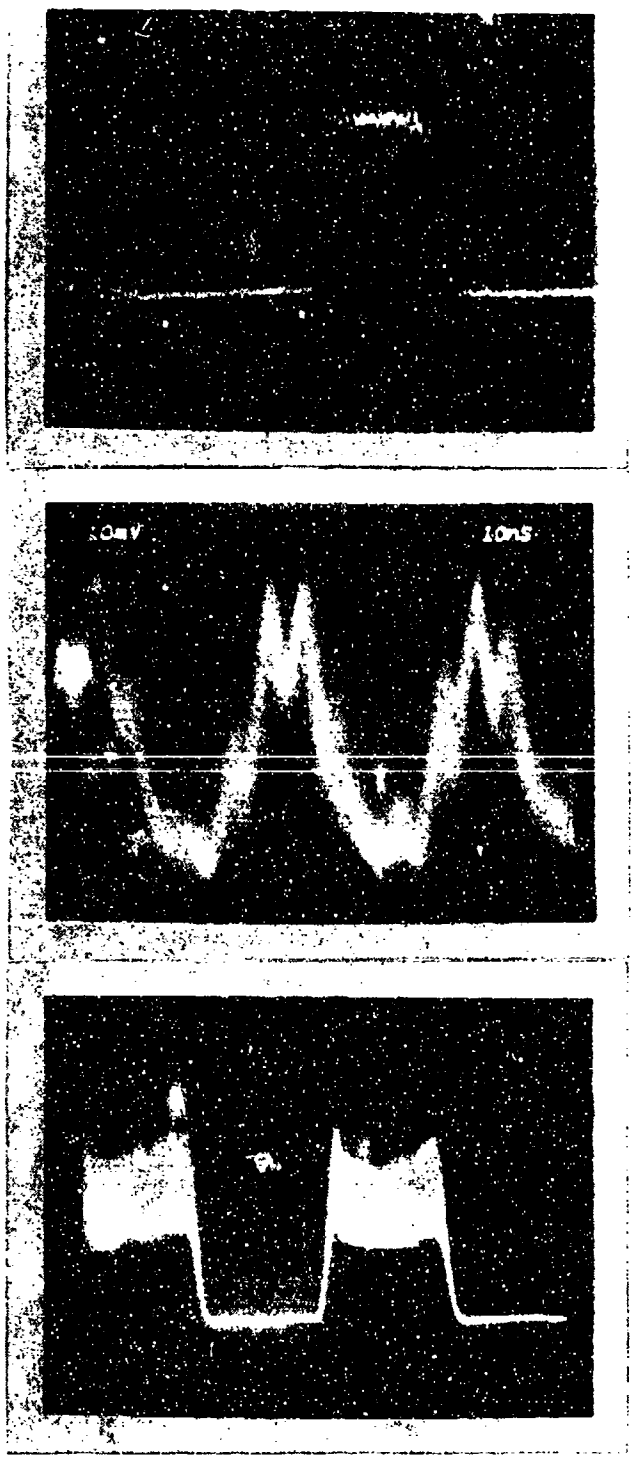

a) Spectrum analyzer trace; center is 20 MHz; 4 MHz/division

b) 500 MHz oscilloscope trace; 10 ns/division

c) 100 MHz oscilloscope trace; 0.2 ms/division

Figure 18. Typical oscilloscope traces of the time-dependent oscillation on a line whose saturated gain does not fill the unstable resonator. These data are for the $P_2(7)$ line for a scraper mirror slit width of 4 mm for the Run 34 flow rates at 5.3 torr. The beam was chopped with a mechanical chopper. The 7 ns mode beat superimposed on the 40 ns oscillation is clearly evident in b.

Run 34
$P_1(7)$

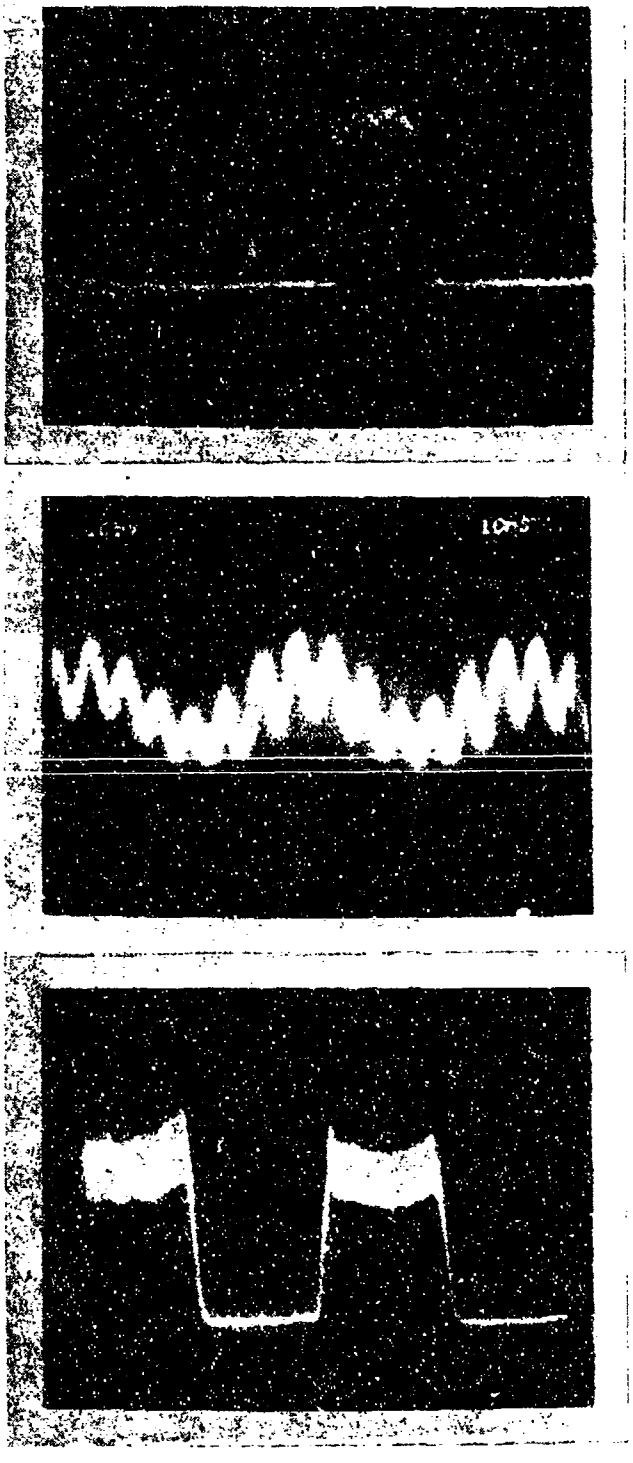

a) Spectrum analyzer trace; center is 20 MHz; 4 MHz/division

b) 500 MHz oscilloscope trace; 10 ns/division

c) 100 MHz oscilloscope trace; 0.2 ms/division

Figure 19. Typical oscilloscope traces of the time-dependent oscillation on a line whose saturated gain does not fill the unstable resonator. These data are for the $P_1(7)$ line for a scraper mirror slit width of 4 mm for the Run 34 flow rates at 5.3 torr. The beam was chopped with a mechanical chopper. The 7 ns mode beat superimposed on the 40 ns oscillation is clearly evident in b.

Run 34
$P_1(8)$

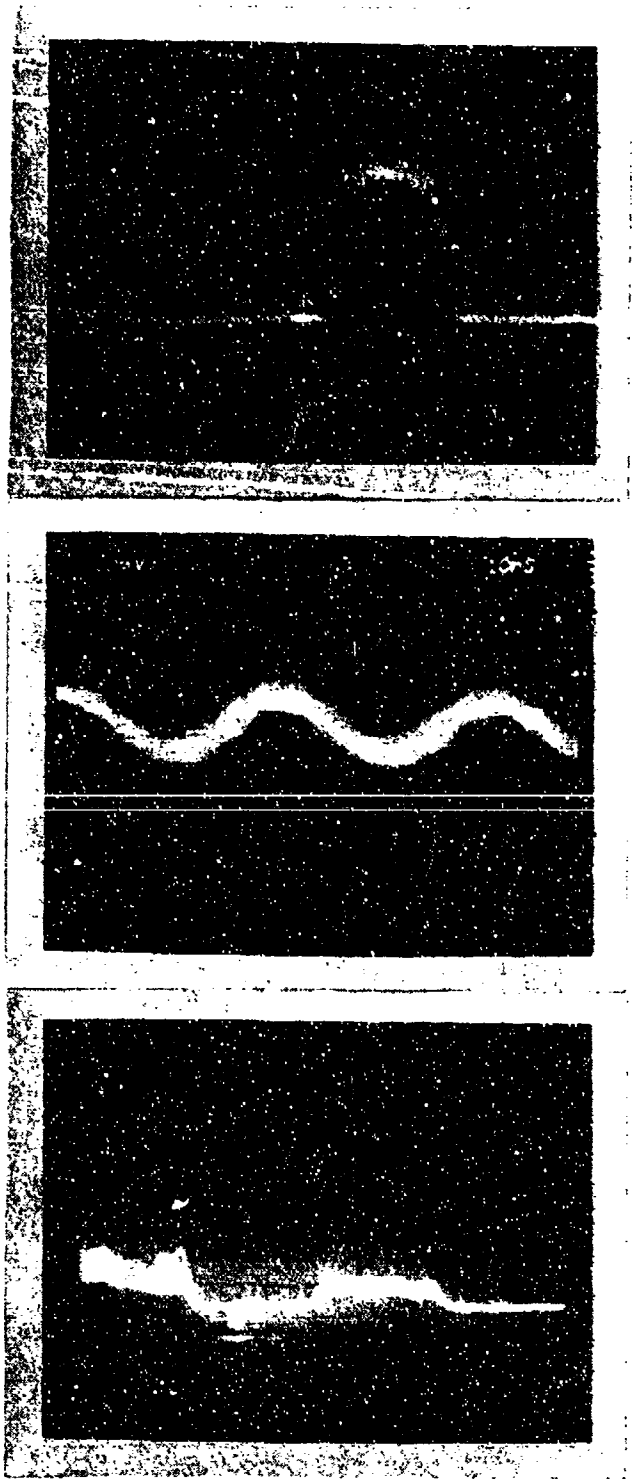

a) Spectrum analyzer trace; center is 20 MHz; 4 MHz/division

b) 500 MHz oscilloscope trace; 10 ns/division

c) 100 MHz oscilloscope trace; 0.2 ms/division

Figure 20. Typical oscilloscope traces of the time-dependent oscillation on a line whose saturated gain does not fill the unstable resonator. These data are for the $P_1(8)$ line for a scraper mirror slit width of 4 mm for the Run 34 flow rates at 5.3 torr. The beam was chopped with a mechanical chopper.

$P_1(8)$. This is evidence that the amplitudes of the time-dependent oscillations are not a function of line strength, which supports the prediction that the amplitudes of the time-dependent oscillations are determined only by the fraction of the resonator filled by the oscillating line.

The details of the 7 ns mode beat, which corresponds to 143 MHz, were not studied because the spectrum analyzer did not extend to 200 MHz.

Comparison of the theoretical calculations for the low pressure Run 34, 5 mm slit case (Section 3.1) and the experimental low pressure Run 34, 4 mm slit data shows that there is qualitative agreement between the calculations and the data. The 5 mm slit calculation is qualitative because the losses introduced by the Brewster windows were not included. The difference in lasing lines between the calculations and the data is due to the omission of the losses introduced by the Brewster windows in the calculation.

3.5 RUN 34, LOW PRESSURE, 2mm SLIT SCRAPER MIRROR DATA

Since the gain distribution is independent of the optical axis location of the resonator[2], as x_c increases, a smaller fraction of the resonator is filled by the saturated gain of the lasing lines. To verify experimentally that the oscillations on lines whose saturated gain does not fill the unstable resonator do not occur for Fresnel numbers less than 1.5, the x_c of the optical axis was varied from 2 mm to 4 mm with the Fresnel number held constant at 1.428 (scraper mirror slit width of 2 mm). Oscillation measurements for the low SF_6 and low H_2 flow rates, Run 34, were taken with the flow control valve wide open, which gave a laser cavity

pressure of 5.3 torr. The data, which are given in Table 6, show that no 40 ns oscillations occurred at any of the x_c locations. Since the saturated gain of the lasing line filled a smaller fraction of the resonator as x_c increased, this result verifies the prediction that the time-dependent oscillations on lines whose saturated gain does not fill the unstable resonator do not occur for Fresnel numbers less than 1.5. The only oscillation that did occur was the 7 ns mode beat.

3.6 RUN 36, LOW PRESSURE, SLIT SCRAPER MIRROR DATA

Oscillation frequency and amplitude measurements for Run 36 flow rates were taken with the flow control valve wide open, which gave a laser cavity pressure of 6.5 torr. Because the resonator was symmetric, the distance between the optical axis and the H_2 injectors was always equal to the scraper mirror slit width. Table 7 is a summary of the oscillation data for the total power as a function of Fresnel number. The MNORO3UR calculations[3] performed prior to the experiment indicated that the period of the oscillations should be 40 ns independent of Fresnel number. From Table 7, it is seen that in addition to the expected 40 ns oscillation, there was a 7 ns oscillation superimposed on top of it. This is the mode beat seen in the Run 34 low pressure data. Table 7 shows that the time-dependent oscillations on lines whose saturated gain did not fill the resonator did not occur for Fresnel numbers below 1.5 and that their amplitude increased as the fraction of the resonator filled by the oscillating line decreased. This data indicates that the time-dependent oscillations on lines whose saturated gain does not fill the resonator are independent of the flow rates.

Run 34 50% Geometric Outcoupled, Symmetric, Confocal, Unstable Resonator
Cavity Pressure 5.3 torr

2 mm Scraper Mirror Slit Width (N_F = 1.428)

x_c mm	Lasing Line	$P_1(4)$	$P_1(5)$	$P_1(6)$	$P_1(7)$	$P_1(8)$	$P_1(9)$	$P_2(5)$	$P_2(6)$	$P_2(7)$	$P_2(8)$	P_T Watts
2.0	OSC Period, ns (Strength of OSC)	-	-	7	7	-		7 (weak)	7	7	-	6.2
3.0	OSC Period, ns (Strength of OSC)			7	7	-		-	7	7 (weak)	-	4.9
4.0	OSC Period, ns (Strength of OSC)			7 (weak)	7	-			7 (weak)	-	-	1.95

- means the line lased but was too weak to operate the fast detector

Table 6. Individual line oscillations for a scraper mirror slit of 2 mm as a function of x_c for Run 34 flow rates at 5.3 torr. A PbSe detector was used to measure time averaged power spectral distributions. Lines too weak to operate the fast InAs detector would operate the PbSe detector.

Run 36 50% Geometric Outcoupled,
Symmetric, Confocal, Unstable Resonator

Scraper Mirror Slit, mm	N_F	P_{cav} Torr	P_T Watts	OSC Period ns	Amplitude Modulation % P_T
1.0	0.357	6.55	7.0		
2.0	1.428	6.5	6.3	7	
3.0	3.214	6.5	3.9	40/7	3.7
4.0	5.714	6.5	1.4	40/7	33.0
5.0	8.929	6.5	0.15	40/7	37.5

Table 7. Frequency and amplitude of the time-dependent oscillation of total power as a function of Fresnel number for the flow rates of Run 36 at 6.5 torr. The SF_6 bottle was running out when these data were taken. This caused the total power to be less than that measured when the individual line oscillation data were taken.

Table 8 presents the oscillation data for individual lines as a function of Fresnel number. From Table 8, it is seen that the 40 ns oscillation on lines whose saturated gain did not fill the resonator did not occur for Fresnel numbers below 1.5. Figure 21 shows typical spectrum analyzer and oscilloscope traces for an oscillating line for Run 36 flow rates at 6.3 torr. Comparison of the traces of Fig. 21 with those of Fig. 19 indicates that the $P_1(7)$ line oscillated with nearly the same amplitude and frequency for both Run 34 and Run 36 flow conditions with a 4 mm slit. This suggests that the length of the saturated gain for the $P_1(7)$ line is approximately the same for both flow rates.

3.7 RUN 34, HIGH PRESSURE, SLIT SCRAPER MIRROR DATA

Oscillation measurements for the low SF_6 and low H_2 flow rates, Run 34, were also taken with the flow control valve partially closed, which gave a laser cavity pressure of 10.1 torr. It was shown in Chapter II that doubling the cavity pressure reduced the length of the saturated gain by approximately a factor of 2. Because the resonator was symmetric, the distance between the optical axis and the H_2 injectors was always equal to the slit width. Table 9 is a summary of the oscillation data for individual lines as a function of Fresnel number. From Table 9 it is seen that the only oscillation observed was the 7 ns mode beat of the laser.

3.8 RUN 36, HIGH PRESSURE, SLIT SCRAPER MIRROR DATA

Oscillation measurements for Run 36 flow rates were also taken with the flow control valve partially closed, which gave a laser cavity pressure of 11.5 torr. Table 10 is a summary of the data. No oscillations were

Run 36 50% Geometric Outcoupled, Symmetric, Confocal, Unstable Resonator
Cavity Pressure 6.3 torr

Scraper Mirror Slit, mm	N_F	Lasing Line	$P_1(4)$	$P_1(5)$	$P_1(6)$	$P_1(7)$	$P_1(8)$	$P_1(9)$	$P_2(5)$	$P_2(6)$	$P_2(7)$	$P_2(8)$	$P_2(9)$	P_T Watts
2.0	1.428	OSC Period, ns (Strength of 7ns OSC)			7	7	-		-	7	7 (weak)	-		6.3
3.0	3.214	OSC Period, ns (Strength of 40ns OSC)			7	40/7 (weak)	40/7 (weak)	-		40/7 (weak)	40/7 (weak)	7	-	4.9
		OSC Freq., MHz				16-28	25-30			18-28	24-30			
4.0	5.714	OSC Period, ns (Strength of 40ns OSC)			-	40/7	40/7	40 (weak)			40/7	40	-	1.9
		OSC Freq., MHz				22-28	23-28	24-28			22-30	22-30		
		Amplitude Modulation $\Sigma P_\nu(J)$				30	50				66	50		
5.0	8.929	OSC Period, ns (Strength of 40ns OSC)				40 (weak)	40/7 (weak)	40/7 (weak)				-	-	0.38-0.40
		OSC Freq., MHz				24-25	24-27	25-27						

- means the line lased but was too weak to operate the fast detector

Table 8. Frequency and amplitude of the time-dependent oscillations on individual lines for the flow rates of Run 36 at 6.3 torr as a function of Fresnel number. A PbSe detector was used to measure time averaged power spectral distributions. Lines too weak to operate the fast InAs detector would operate the PbSe detector.

Run 36
$P_1(7)$

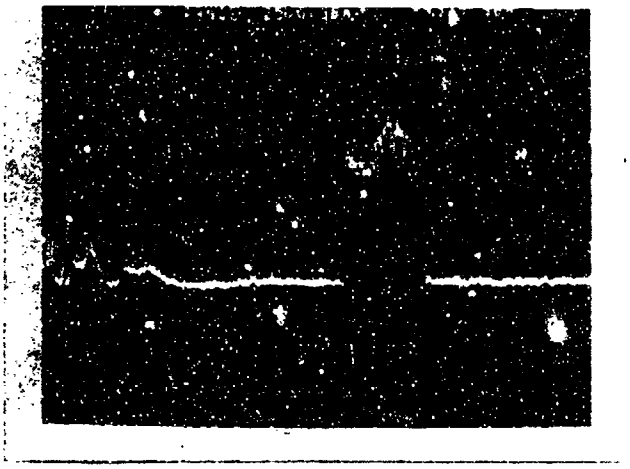

a) Spectrum analyzer trace;
center is 20 MHz;
4 MHz/division

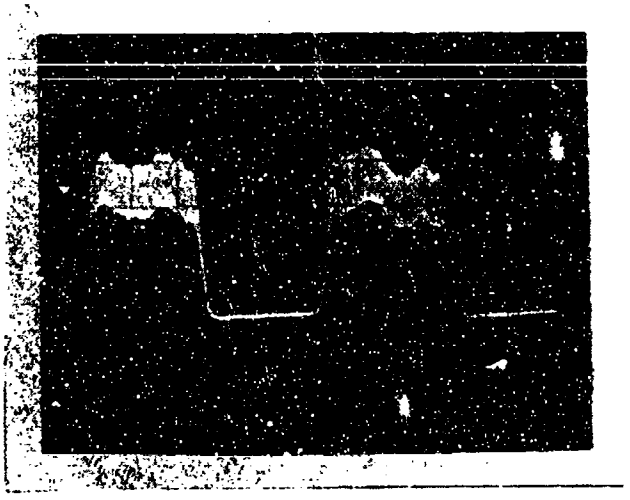

b) 100 MHz oscilloscope trace;
0.2 ms/division

Figure 21. Typical oscilloscope traces of the time-dependent oscillation on a line whose saturated gain does not fill the unstable resonator. These data are for the $P_1(7)$ line for a scraper mirror slit width of 4 mm for the Run 36 flow rates at 6.3 torr. The beam was chopped with a mechanical chopper.

Run 34 50% Geometric Outcoupled, Symmetric, Confocal, Unstable Resonator
Cavity Pressure 10.1 torr

Scraper Mirror Slit, mm	N_F	Lasing Line	$P_1(5)$	$P_1(6)$	$P_1(7)$	$P_1(8)$	$P_1(9)$	$P_2(5)$	$P_2(6)$	$P_2(7)$	$P_2(8)$	P_T Watts
1.0	0.357	OSC Period, ns		-					-	-		1.15
2.0	1.428	OSC Period, ns			7	-				-	-	1.10
3.0	3.214	OSC Period, ns			-	-	-					0.15
4.0	5.714	OSC Period, ns										0.0

- means the line lased but was too weak to operate the fast detector

Table 9. Individual line oscillations for the flow rates of Run 34 at 10.1 torr as a function of Fresnel number. A PbSe detector was used to measure time averaged power spectral distributions. Lines too weak to operate the fast InAs detector would operate the PbSe detector.

Run 36: 30% Geometric Outcoupled, Symmetric, Confocal, Unstable Resonator

Scraper Slit, mm	Mirror	N_F	P_{cav} Torr	P_T Watts	OSC Period ns
1.0		0.357	11.5	2.0	none
2.0		1.428	11.5	0.925	none
3.0		3.214	11.5	0.0	
4.0		5.714	11.5	0.0	
5.0		8.929	11.5	0.0	

Table 10. Frequency and amplitude of the time-dependent oscillation of total power as a function of Fresnel number for the flow rates of Run 36 at 11.5 torr.

observed for any of the Fresnel numbers tested. The absence of lasing for the 5 mm slit case verifies the MNORO3UR calculation[3] for Run 36 at 11.5 torr with a 5 mm slit scraper mirror which showed that lasing would not occur.

Since the time-dependent oscillations are a consequence of rotational nonequilibrium and do not occur if rotational equilibrium is maintained[1], these oscillations may not occur as the rotational relaxation rate increases as the pressure in the laser cavity increases. The absence of the time-dependent oscillations in the high pressure cases may thus be a consequence of the increased rotational relaxation rate which occurs at the higher pressure. On the other hand, the absence of these oscillations in the high pressure cases may be a consequence of the short gain zones[2,5,6,7] (< 3 mm) which result in the Fresnel number (based on the saturated gain zone lengths) being less than 1.5, which is too small for the time-dependent oscillations to occur. To investigate these possibilities, the laser should be run with the flow control valve wide open to obtain the highest possible flow velocity, and consequently the longest saturated gain zones possible, with the flow rates increased until the pressure is in the 10 to 12 torr range. If the measured beam diameters are in the 4 mm to 5 mm range for these conditions and the time-dependent oscillations do not occur at the 10 to 12 torr pressure range, the data may then indicate that the increased rotational relaxation rate at these pressures is the responsible mechanism. MNORO3UR modeling calculations should be performed to assist in the interpretation of the data.

3.9 RUN 34, LOW PRESSURE, RECTANGULAR HOLE SCRAPER MIRROR DATA

Measurements of the time-dependent oscillations were made for the confocal unstable resonator with a rectangular hole scraper mirror. In this case the resonator is a three dimensional, 75% geometric outcoupled, confocal unstable resonator rather than a strip resonator, as is the case when the variable slit scraper mirror is used. The hole in the scraper mirror is 1.5 mm high by 7.07 mm long, which corresponds to an effective width of 5.0 mm in the flow direction. This resonator outcoupled a large percentage of the power from the top and bottom edges of the scraper mirror rather than from the upstream-downstream edges, which was the only way the variable slit scraper mirror could outcouple the power.

Oscillations were observed for the Run 34 flow rates at 5.2 torr with the rectangular hole scraper mirror as a function of x_c. Table 11 is a summary of the data. The data were obtained from 500 MHz oscillocope traces. Unfortunately, the 40 MHz spectrum analyzer, which had been borrowed from another research group, was not available at the time of these experiments. Table 11 shows that the time-dependent oscillations do occur when a 3-D resonator is used. The periods of the oscillations agree with the predicted 40 ns period. In addition to the 40 ns time-dependent oscillation, the 7 ns mode beat was also observed. Fig. 22 shows typical 500 MHz oscilloscope traces for two of the oscillating lines. Fig. 22a shows the 40 ns oscillation and Fig. 22b shows the 7 ns mode beat of the laser. These data show that the period of the oscillations is independent of the dimensionality of the resonator.

The time-dependent oscillations had the same frequency for both the 2-D and 3-D unstable resonators. This suggests that the frequency of the

Run 34 75% Geometric Outcoupled, Confocal, Unstable Resonator
(Rectangular Hole Scraper Mirror)
Cavity Pressure 5.2 torr N_F = 8.929

x_c	Oscillating Line	$P_1(6)$	$(P_1(7)$	$P_1(8)$	$P_2(5)$	$P_2(6)$	$P_2(7)$	$P_2(8)$	P_T
mm									Watts
2.0	OSC Period, ns	7	44/7	47/7	46/7		52/7	49/7	5.5
	OSC Freq., MHz		23	21	22		19	21	
3.0	OSC Period, ns	45/7	42/7	43	42	44-39/7	42/7	41/7	7.0
	OSC Freq., MHz	22	24	23	24	23-26	24	24	
4.0	OSC Period, ns	44/8	42/7	43	41	43	42/7	41	6.3
	OSC Freq., MHz	23	24	23	24	23	24	24	
5.0	OSC Period, ns	45	42/7	42/7	42/7	46	7	40	
	OSC Freq., MHz	22	24	24	24	22		25	
5.5	OSC Period, ns				37		7		
	OSC Freq., MHz				27				
6.0	OSC Period, ns	48	7						
	OSC Freq., MHz	21							

Table 11. Period and frequency of the time-dependent oscillations on individual lines for a scraper mirror with a rectangular hole 1.5 mm high by 7.07 mm long (corresponding to an effective slit of 5.0 mm in the flow direction), for Run 34 flow rates at 5.2 torr as a function of x_c. Total powers were not recorded for the 5 mm, 5.5 mm and 6 mm slit widths.

Run 34
Rectangular Hole
Scraper Mirror

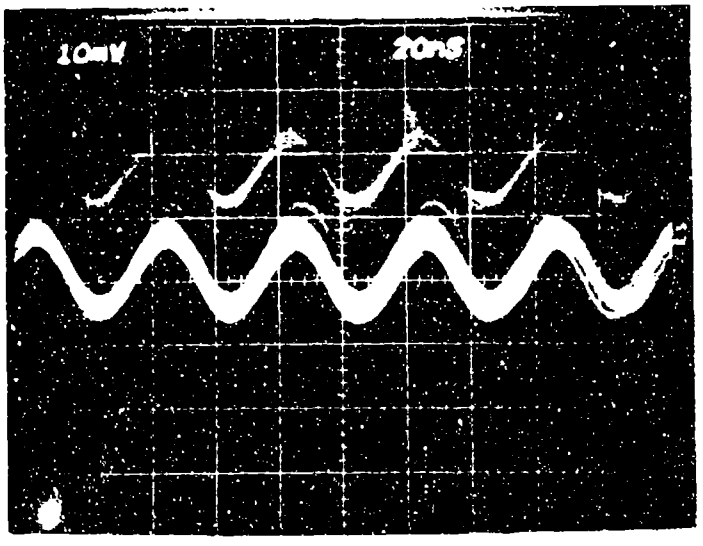

a) $P_2(8)$;
500 MHz oscilloscope trace; 20 ns/division, showing the 40 ns time-dependent oscillation

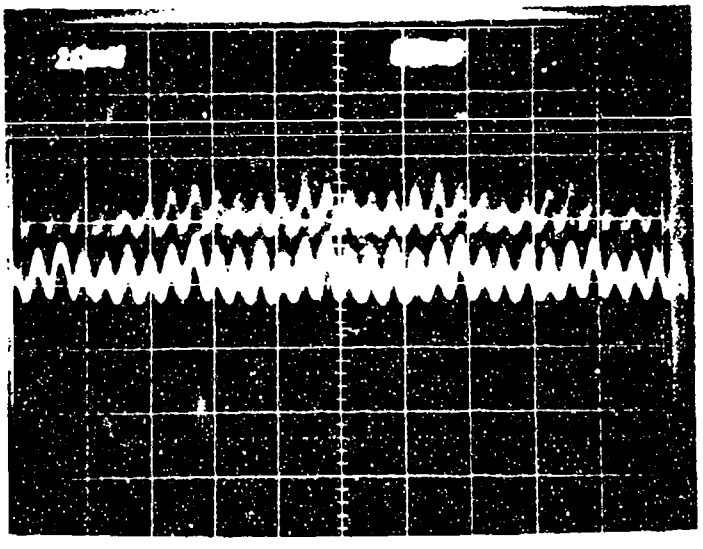

b) $P_1(7)$;
500 MHz oscilloscope trace; 20 ns/division, showing the 7 ns mode beat of the laser

Figure 22. Typical oscilloscope traces of the time-dependent oscillations on lines whose saturated gain does not fill the unstable resonator. These data are for the lines $P_2(8)$ and $P_1(7)$ for a scraper mirror with a rectangular hole 1.5 mm high by 7.07 mm long (corresponding to an effective slit of 5.0 mm in the flow direction), for the Run 34 flow rates at 5.2 torr. The optical axis of the resonator was at the center of the hole in the scraper mirror. The beam was chopped with a mechanical chopper.

time-dependent oscillation is a function of magnification not geometric outcoupling, because both the 2-D and 3-D resonators had the same magnification of 2, but the 2-D resonator had a geometric outcoupling ratio of 50% while the 3-D resonator had a geometric outcoupling ratio of 75%. The magnification of the unstable resonator should be changed to determine whether the frequency of the time-dependent oscillation changes as predicted[1,2].

Unfortunately, the rectangular hole scraper mirror could not be aligned as accurately as the slit scraper mirror because of the difficulty of determining when the HeNe alignment beam was at the center of the hole. Thus, there was uncertainty in the location of the scraper mirror with respect to the optical axis. In spite of this alignment problem, the data with the rectangular hole scraper mirror show that the time-dependent oscillations on lines whose saturated gain does not fill the unstable resonator occur in 3-D as well as 2-D resonators. Further work needs to be done to determine the extent of the 3-D effect on the total power, spectra and time-dependent oscillations for the various flow conditions.

IV. CONCLUDING REMARKS

The comparison of the low pressure stable resonator data with the corresponding high pressure data showed that the beam diameter and total power increased for all six flow rate combinations when the cavity pressure was decreased. The total power increases are evidence that the HF deactivation rate decreased due to the lower pressure. The fraction of the power in the 1→0 vibrational band did not change significantly for any of the flow rates when the pressure was decreased. The power spectral distributions shifted to lower J's as the pressure decreased, due to the decrease in rotational relaxation which occurs at low pressures. The comparison of the MNORO3 power spectral distributions with the low pressure stable resonator data showed that the model is in reasonable agreement with the data. As in the high pressure case, the predicted peak of the power spectral distribution was one or two J's too low. The difference between the MNORO3 predictions and the experimental stable resonator data is a consequence of the Fabry-Perot resonator employed in the calculations. Since, for the high pressure case, the stable resonator model, MNORO3SR, power spectral distributions were in better agreement with the data, a similar result is expected for the low pressure case. These comparisons show that the model agrees with the data as flow rates, cavity losses and pressure are varied.

The minimum in the spectra at $P_2(11)$ occurred in the low pressure as well as in the high pressure data. However, the lines $P_2(10)$ to $P_2(12)$ were weaker in the low pressure cases than in the high pressure cases. This supports the interpretation of the minima as evidence of a kinetic effect, namely a near resonant energy transfer fr m v=3, J=3, 4 to v=2,

J=14 with a subsequent rotational cascade to v=2, J=11.

The time-dependent oscillations in the output power of a cw laser employing a confocal, unstable resonator all had a period of about 40 ns and increased in amplitude as the fraction of the resonator filled by the saturated gain of the oscillating line decreased. The period of the oscillation is independent of flow conditions and the amplitude of the oscillation depends only upon the fraction of the resonator filled by the oscillating line, as predicted by the MNORO3UR calculations. There was a strong cascade coupling between the oscillating 2→1 and 1→0 lines. In addition to the 40 ns oscillation, a 7 ns oscillation was observed superimposed on top of it. The 7 ns oscillation probably corresponds to a mode beat of the laser. As predicted by the MNORO3UR calculations, the oscillations on lines whose saturated gain did not fill the unstable resonator do not occur for Fresnel numbers less than 1.5.

The time-dependent oscillations did not occur for the high pressure cases which may be either a consequence of the increased rotational relaxation rate which occurs at higher pressure or the saturated gain zones may be too short, which causes the Fresnel number (based on the saturated gain zone lengths) to be too small for the time-dependent oscillations to occur. To investigate these possibilities, the laser should be run at high pressure with a high flow velocity to stretch the saturated gain zones sufficiently (Fresnel number > 3) to determine whether the time-dependent oscillations occur at high pressure.

Time-dependent oscillations on lines whose saturated gain did not fill the unstable resonator were also observed using a scraper mirror with a rectangular hole in it. The periods and amplitudes were similar to those

which occurred using the split scraper mirror. Thus, the time-dependent oscillations occur in both two and three dimensional unstable resonators.

The data indicated that the frequency of the time-dependent oscillations is determined by the resonator magnification rather than the geometric outcoupling ratio. The resonator magnification should be changed to determine whether the frequency of the time-dependent oscillations changes as predicted[1,2].

By varying the optical axis location of the unstable resonator and noting when various lines begin to exhibit the time-dependent oscillations, it may be possible by comparison with the MNOR03UR gain profiles to determine the extent of the saturated gain zones in the unstable resonator. If this procedure would work, the occurrence of the time-dependent oscillations could be developed into a diagnostic technique for measuring the extent of the saturated gain zones of the lasing lines in the unstable resonator. Such a capability would represent a significant increase in the level of diagnostic detail obtainable from a chemical laser and would greatly increase confidence in design calculations.

REFERENCES

1. L. H. Sentman, "Chemical Laser Power Spectral Performance: A Coupled Fluid Dynamic, Kinetic and Physical Optics Model," Applied Optics, 17, 2244, 1978.

2. L. H. Sentman, W. O. Mosebach and P. Renzoni, "A Theoretical and Experimental Study of cw Chemical Laser Performance," AAE 81-8, UILU Eng. 81-0508, University of Illinois, Urbana, IL, December 1981.

3. L. H. Sentman, P. F. Schmidt and G. M. Marinos, "Effects of the HF Rate Package and the Optical Resonator on cw HF Chemical Laser Performance," AAE TR 83-6, UILU Eng. 83-0506, Aeronautical and Astronautical Engineering Dept., University of Illinois, Urbana, IL, June 1983.

4. E. B. Turner, R. A. Chodzko and H. Mirels, "Temporal Stability of Single Line cw HF Chemical Laser with Unstable Resonator," J. of Applied Phys., 48, 1163, 1977.

5. L. H. Sentman, M. H. Nayfeh, W. O. Mosebach, P. Renzoni, K. Herrick, K. King, P. Schmidt and S. Townsend, "Theoretical and Experimental Study of cw HF Chemical Laser Performance," Proceedings of the 4th International Symposium on Gas Flow and Chemical Lasers, Stresa, Italy, September 13-17, 1982, Plenum Publishing Corp., NY, in press.

6. L. H. Sentman, P. Renzoni, S. Townsend, M. H. Nayfeh and K. K. King, "The Effects of Cavity Losses on the Performance of a Subsonic cw HF Chemical Laser," TR AAE 83-7, UILU Eng. 83-0507, Aeronautical and Astronautical Engineering Dept., University of Illinois, Urbana, IL, June 1983.

7. L. H. Sentman, M. H. Nayfeh, P. Renzoni, K. King, S. Townsend and G. Tsioulos, "Saturation Effects in a cw HF Chemical Laser," AIAA Paper

84-1576, 17th Fluid Dynamics, Plasmadynamics and Laser Conference, Snowmass, CO, June 25-27, 1984.

8. J. W. Raymonda, M. Subbiah, J. T. Schimke, S. W. Zelazny and L. H. Sentman, "Advanced HF and DF Chemical Laser Performance Modeling, Vol. I, The CNCDE/BLAZE Rotational Equilibrium Code," TR DRCPM HEL-CR-79-7, Bell Aerospace Textron, Buffalo, NY, 1979.

9. L. H. Sentman and P. Schmidt, "MNORO3: An Efficient Rotational Nonequilibrium cw HF Chemical Laser Model," TR AAE 83-1, UILU Eng. 83-0501, Aeronautical and Astronautical Engineering Dept., University of Illinois, Urbana, IL, January 1983.

10. L. H. Sentman and W. Brandkamp, "An Efficient Rotational Nonequilibrium Model of a cw Chemical Laser," TR 79-5, UILU Eng. 79-0505, Aeronautical and Astronautical Engineering Dept., University of Illinois, Urbana, IL, July 1979.

11. J. T. Schmike, "Numerical Model Development for Laser Cavity Flowfields," Bell Aerospace Textron, Report 9278-950002, Buffalo, NY, November 1979.

12. Fresnel number $N = D^2/4 \lambda L$ where D is the mirror diameter, λ is the wavelength and L is the mirror spacing.

13. S. W. Townsend and L. H. Sentman, "Design of a Constant Efficiency Spectrometer for IR Wave Lengths," Applied Optics, in press.